Progress in Oceanography 138 (2015) 399–416

Contents lists available at ScienceDirect

Progress in Oceanography

journal homepage: www.elsevier.com/locate/pocean

# Simulating anchovy's full life cycle in the northern Aegean Sea (eastern Mediterranean): A coupled hydro-biogeochemical–IBM model

D. Politikos [a,1], S. Somarakis [b,1], K.P. Tsiaras [a,1], M. Giannoulaki [b], G. Petihakis [a], A. Machias [b], G. Triantafyllou [a,*]

[a] Hellenic Centre for Marine Research, Institute of Oceanography, Greece
[b] Hellenic Centre for Marine Research, Institute of Marine Biological Resources and Inland Waters, Greece

ARTICLE INFO

*Article history:*
Available online 11 September 2014

ABSTRACT

A 3-D full life cycle population model for the North Aegean Sea (NAS) anchovy stock is presented. The model is two-way coupled with a hydrodynamic–biogeochemical model (POM–ERSEM). The anchovy life span is divided into seven life stages/age classes. Embryos and early larvae are passive particles, but subsequent stages exhibit active horizontal movements based on specific rules. A bioenergetics model simulates the growth in both the larval and juvenile/adult stages, while the microzooplankton and mesozooplankton fields of the biogeochemical model provide the food for fish consumption. The super-individual approach is adopted for the representation of the anchovy population. A dynamic egg production module, with an energy allocation algorithm, is embedded in the bioenergetics equation and produces eggs based on a new conceptual model for anchovy vitellogenesis. A model simulation for the period 2003–2006 with realistic initial conditions reproduced well the magnitude of population biomass and daily egg production estimated from acoustic and daily egg production method (DEPM) surveys, carried out in the NAS during June 2003–2006. Model simulated adult and egg habitats were also in good agreement with observed spatial distributions of acoustic biomass and egg abundance in June. Sensitivity simulations were performed to investigate the effect of different formulations adopted for key processes, such as reproduction and movement. The effect of the anchovy population on plankton dynamics was also investigated, by comparing simulations adopting a two-way or a one-way coupling of the fish with the biogeochemical model.



## Introduction

Small pelagic fish (SPF), such as anchovy and sardine, comprise species that are plankton feeders, playing an important role in marine food webs as they are the principal means of transferring production from plankton to larger predators, including marine mammals and seabirds (Fréon et al., 2005). Fishing these species can have large impacts on other groups (vertebrate, invertebrate, primary and secondary producers) of the ecosystem (Smith et al., 2011). In addition, SPF have a short life span, high fecundities and by feeding on the plankton-based food chains, they respond rapidly to changes in ocean conditions (Alheit et al., 2009). Thereby, they are extremely variable in their abundance at both inter-annual and inter-decadal scales (Alheit et al., 2009). An effective management system for these resources would need to incorporate an understanding of the mechanisms that control the variations in abundance, distribution and productivity of the populations, as well as the ecosystem interactions and feedbacks these variations may set in motion. Furthermore, the extreme variability that characterizes the SPF recruitment implies that traditional fishery management measures, based on estimates of long term average yield from stock assessment, may not be effective in preventing episodes of serious overfishing (Fréon et al., 2005). There is an increasing need to understand how physics, biogeochemistry and biology combine to produce the observed patterns of population variability and to enhance ecosystem considerations in the management of the SPF resources by developing state-of-the-art end-to-end models (Fulton, 2010; Rose et al., 2010).

The European anchovy (*Engraulis encrasicolus*) is one of the most important SPF in the Mediterranean Sea. Three major stocks exist in the basin, supporting the largest SPF fisheries in the area. These stocks inhabit the NW Mediterranean (Catalan Sea and Gulf of Lions), the Adriatic Sea and the northern Aegean Sea (Somarakis et al., 2004). The above areas are characterized by wide continental shelves, exceptionally higher productivity, in relation to the highly oligotrophic character of other Mediterranean regions and

* Corresponding author.
*E-mail address:* gt@hcmr.gr (G. Triantafyllou).
[1] These authors contributed equally to this paper.

http://dx.doi.org/10.1016/j.pocean.2014.09.002
0079-6611/

favorable conditions for larval survival (Agostini and Bakun, 2002). Moreover, these suitable anchovy habitats are spatially restricted and separated from each other by deep, extremely oligotrophic basins, which would not be likely to support anchovy feeding and reproduction (Somarakis et al., 2004). For example, in our case study area, i.e. the Aegean Sea, there is a sharp contrast in productivity between its northern and southern basin and anchovy schools are practically absent from the later (Stergiou et al., 1997). Anchovies remain close to the areas of higher productivity and many density dependent controls have been identified such as on plankton consumption (Nikolioudakis et al., 2014), daily egg production (Somarakis et al., 2012) and larval mortality (Somarakis and Nikolioudakis, 2007).

End-to-end models (E2E) provide today a thriving approach in marine ecosystem dynamics. They attempt to unify the different levels of the food web from climate to lower trophic levels to fish and fisheries (Travers et al., 2007; Rose et al., 2010). Numerous biophysical modelling studies have contributed to a better understanding of fish dynamics and their ecological response to climate change and management actions (Travers et al., 2007; Lett et al., 2009; Hinrichsen et al., 2011; Ito et al., 2013). A full life cycle fish model was developed by Huse and Ellingen (2008) to represent the migration, spatial and population dynamics of capelin in the Barents Sea. The model was then used to perform simulations with present day climate and a future climate scenario. The climate warming scenario showed a shift in the adult distribution, with a parallel shift of spawning habitats and an earlier starting of spawning activity. In the North Western Pacific, a two-dimensional individual-based fish model was developed to evaluate the effect of movement on the recruitment success of Japanese sardine (Okunishi et al., 2012). For Pacific saury, Ito et al. (2013) investigated the fish growth response under global warming scenarios using an ecosystem-based bioenergetics/migration model. Simulations predicted future shifts in size distribution and abundance of saury, contributing to a more comprehensive understanding of fish responses to climate change.

The development of a full life cycle model for a small pelagic fish needs a complex, multi-step approach. It requires knowledge on a suite of processes (growth, spawning and movement strategy, planktonic prey selection), during the course of fish development (Huse and Ellingen, 2008; Wang et al., 2013). A 3-D IBM was developed for the first time in the North Aegean Sea (NAS, eastern Mediterranean, (Fig. 1)) by coupling the full life cycle of anchovy (from eggs to adults) with a 3-D hydrodynamic–biogeochemical lower trophic level model (LTL). The IBM consists of several modules: the bioenergetics approach (Mukai et al., 2007; Politikos et al., 2011) is used to simulate anchovy growth and reproduction under seasonally varying food and temperature conditions, provided by the LTL model. The anchovy population is controlled by natural and fishing mortalities, which are updated as the fish pass through successive life stages. Physical and biological cues determine fish advection/movement. Finally, an energy allocation algorithm, based on the approach of Pecquerie et al. (2009), is used to control egg production, taking into account all basic characteristics of anchovy spawning strategy in the NAS.

Once the IBM model was coupled and tuned, it was then used to simulate the anchovy population dynamics in the NAS through an interannual hindcast simulation for the period 2003–2006. The simulated somatic growth, population biomass and egg production were compared with available field data, derived mainly from acoustic and daily egg production (DEPM) surveys, carried out during early summer in the same period (2003–2006). Additional sensitivity simulations were performed to investigate the effect of different formulations adopted for key processes, such as reproduction and movement. Finally, through the two-way coupling of the fish with the LTL model, the effect of the anchovy population on plankton dynamics was also investigated.

## Materials and methods

### *Lower trophic model (LTL)*

The three-dimensional, coupled lower trophic model used in this study has been developed for the NAS ecosystem, as described in Tsiaras et al. (2012) and Tsiaras et al. (2014). It consists of a hydrodynamic model, based on POM (Princeton Ocean Model; Blumberg and Mellor, 1983) and a comprehensive biogeochemical model, based on ERSEM (European Regional Seas Ecosystem Model, Baretta et al., 1995; Petihakis et al., 2002). Both models are widely used in the scientific community and have been previously implemented in the area (Kourafalou and Tsiaras, 2007; Politikos et al., 2011; Tsiaras et al., 2010; Tsiaras et al., 2012, 2014). The biogeochemical component has been adopted from Petihakis et al. (2002), being further calibrated and validated against remote sensing and in situ data (Politikos et al., 2011; Tsiaras et al., 2014). ERSEM may be characterised as generic, following the functional group approach, where organisms are separated according to their trophic role (producers, consumers, etc.) and subdivided according to their size (Fig. 2). Organic carbon is produced and transferred within the trophic web through physiological and population processes, while variable nutrient pools of nitrogen, phosphorus and silicate are dynamically coupled with the carbon dynamics. Briefly, there are four groups of primary producers, ranging from the very small picophytoplankton (<2 μm) to the significantly larger diatoms and dinoflagellates (20–200 μm). There are also three zooplanktonic groups (heterotrophic nanoflagellates, microzooplankton, mesozooplankton) that each feed on more than one food source among phytoplankton and bacteria groups (Fig. 2). A significant advantage of this particular model is the detailed description of the microbial food web, which is particularly suitable for the simulation of the most important ecosystem characteristics within the environment of the Eastern Mediterranean. For more details on the biophysical model description, the interested reader can refer to Petihakis et al. (2002), Kourafalou and Tsiaras (2007) and Tsiaras et al. (2012, 2014). The LTL model domain is shown in Fig. 1. The horizontal resolution is 1/10° (~10 km), while 25 sigma-levels are resolved in the vertical, with logarithmic distribution approaching the surface.

### *Anchovy IBM model*

#### *Life cycle stages and age classes*

Anchovies are considered to have a maximum lifespan of 3.5 years (Somarakis et al., 2006), which is divided into seven life stages/age classes. The length thresholds and reference dates for the transition from one life stage/age class to the next are shown in Table 1. Specifically, the early life history (ELS) is divided into three stages according to length: (a) embryonic (egg + yolk sac larvae) (<3.5 mm, autotrophic stage), (b) early larval (<11 mm) and (c) late larval stage (11–42 mm).

The various stages of anchovy's life history were based on documented differences in feeding preferences and movement capabilities. The first two stages (<11 mm, i.e. egg, yolk sac, preflexion and early postflexion larvae) have limited swimming capabilities, un-developed vertical migration behaviour and feed on microzooplankton (Somarakis and Nikolioudakis, 2010). Late larval and juvenile stage anchovies have developed significant behavioural and swimming capabilities and are able to respond effectively to physical transport. Vertical migration behaviour has been fully developed by these stages, while a shift in feeding preferences from microzooplankton to mesozooplankton is taking place during the late larval stage (Nikolioudakis, 2011).

Although length at 50% maturity of the NAS anchovy is 105 mm (Somarakis et al., 2006), it was more convenient to adopt a reference

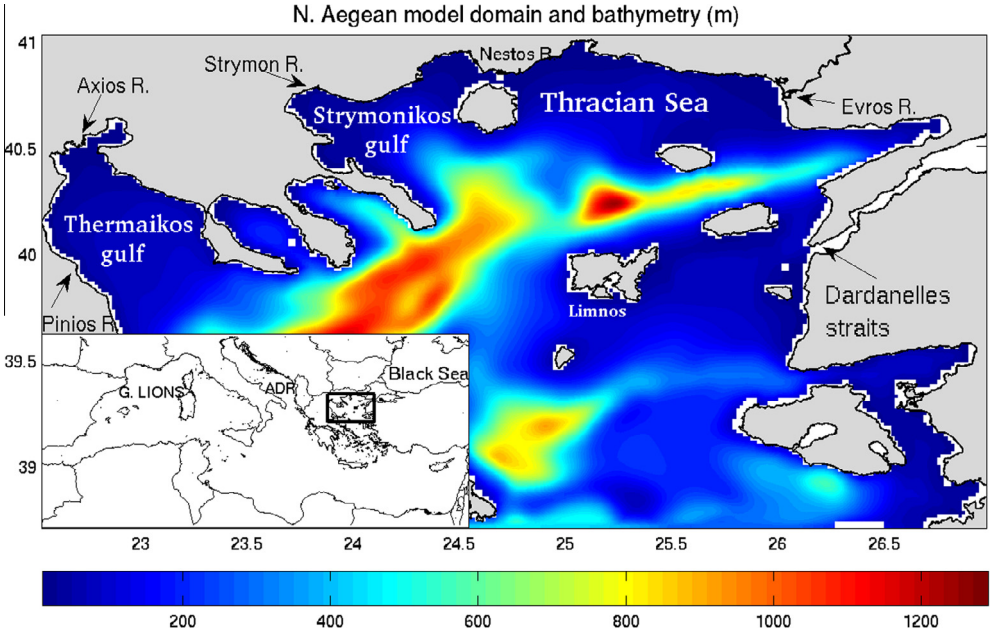


**Fig. 1.** North Aegean Sea (NAS) model domain and bathymetry. Major NAS rivers and the Dardanelles Strait are indicated.

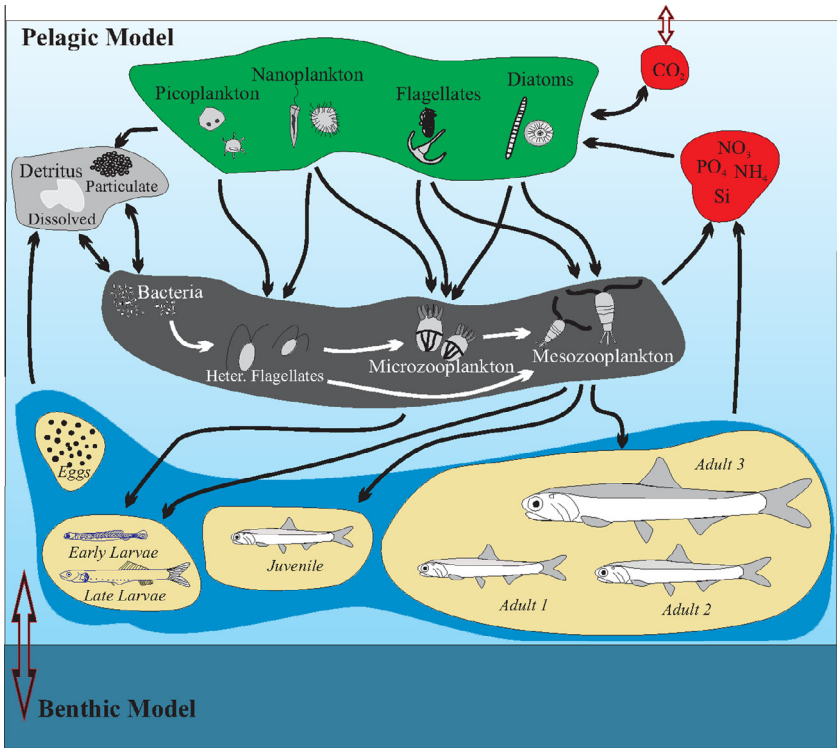


**Fig. 2.** Schematic diagram of the anchovy IBM model coupled with the LTL model.

date for the transition from the juvenile to the adult stage or from one adult age group to the next, given the extended spawning period from May to September (Somarakis et al., 2006) and the high variability in individual growth rates (Uriarte et al., 1996; Somarakis et al., 2006). The 1st of March was selected as the appropriate date (Table 1) because it coincides with the start of the annual fishing period for purse seines and matches closely the onset of the gonadal maturation in spring (Schismenou et al., 2012).

*Super individuals*

The super-individual (SI) approach is adopted for the representation of the anchovy population (Scheffer et al., 1995). The attributes that characterize the SIs are: life stage/age class, weight (g), length (mm), age (day) and position (longitude, latitude). SIs that belong at the same life stage or age class have identical characteristics in terms of feeding preferences, mortalities and behavioural movement.

**Table 1**
Length ranges and reference dates for life history stage and age class transitions applied within the IBM model.

| Stage/Age class | Length/Date |
|---|---|
| Embryonic stage ($j = 1$) | <3.5 mm |
| Early larval stage ($j = 2$) | 3.5–11 mm |
| Late larval stage ($j = 3$) | 11–42 mm |
| Juvenile stage, age-0 ($j = 4$) | 42 mm – 1st March |
| Adult stage, age-1 ($j = 5$) | 1st March–28th February |
| Adult stage, age-2 ($j = 6$) | 1st March–28th February |
| Adult stage, age-3 ($j = 7$) | 1st March–1th September |

*Bioenergetics*

For the simulation of the anchovy growth, the Wisconsin bioenergetics framework (Mukai et al., 2007; Rose et al., 2007) has been adopted. A one-way coupling configuration to a 1-D version of the biophysical model has been already implemented in the NAS (Politikos et al., 2011). The same model is used here with appropriate adaptations for the 3-D case.

The wet weight increment per unit weight of a SI is calculated by the equation:

$$\frac{1}{W_{SI}} \cdot \frac{dW_{SI}}{dt} = [C - (R + EG + SDA + EX + RE)] \cdot \frac{CAL_z}{CAL_f}, \quad (1)$$

where $W_{SI}$ = fish wet weight (g), $t$ = time (days), $C$ = consumption, $R$ = respiration (or losses through metabolism), $EG$ = egestion (or losses because of faeces), $SDA$ = dynamic action (or losses because of energy costs of digesting food), $EX$ = excretion (or losses of nitrogenous excretory wastes) and $RE$ = the energy allocated to reproduction. Components of the energy budget ($C$, $R$, $EG$, $EX$, $SDA$, $RE$) are in units of (g prey g fish$^{-1}$ day$^{-1}$), which are converted to (g fish g fish$^{-1}$ day$^{-1}$) by using $CAL_z$ = caloric equivalent of zooplankton (cal g prey$^{-1}$) and $CAL_f$ = caloric equivalent of fish (cal g fish$^{-1}$). The g of prey and fish refer both to wet weight. The two LTL plankton groups that were considered as prey types for anchovy are mesozooplankton and microzooplankton (Table A.1). The components of Eq. (1) and the related parameters (except from prey vulnerabilities and half saturations) were adopted from Politikos et al. (2011) and are summarized in Table A.1. The piecewise length–weight relationship estimated in Politikos et al. (2011) is used to convert weight to length. Eq. (1) is solved every 20 min (the IBM has the same time step with the LTL model).

In the 3-D version of the bioenergetics model, prey vulnerabilities, which parameterize the feeding preferences, were re-adjusted and half saturation constants $k$ were re-calibrated to provide the best fit between the simulated and observed anchovy growth (Table A.1). To account for satiation (cessation of ingestion when having eaten much) and realistically represent the juvenile and adult growth in cases of increased plankton abundances, a maximum of 6% of fish weight was imposed for daily consumption. The rational of selecting this value was that in all studies measuring the daily ration of small pelagic fish, the daily consumption estimates were lower than 6% of fish weight (Palomera et al., 2007; Nikolioudakis, 2011). It is assumed that when the fish reaches this maximum, it stops feeding for the rest of the day.

Both, in the early and adult stages a starvation condition threshold is also imposed, below which the SI vanishes. It is assumed that there is a limit of 35% in cumulative weight loss, corresponding to the weight estimated from the length–weight relationship. This limit was set empirically, after examining the available length–weight relationships for larval, juvenile and adult anchovy (Fig. B.1). In all cases, residuals of the length weight relationship were <35% of predicted weight. A similar estimation for starvation status was also used by Oguz et al. (2008) to simulate the anchovy population dynamics in the Black Sea.

A new egg production scheme was developed to include the dynamic process of energy allocation to reproduction $RE$ and growth. This component of the model is described in a following section.

*Population dynamics*

The number of individuals within each anchovy SI is reduced due to natural and fishing mortality,

$$\frac{dN_{SI}}{dt} = -(M_{SI} + F_{SI})N_{SI},$$

where $N_{SI}$ denotes the number of individuals within the SI, $M_{SI}$ is the assigned natural mortality rate and $F_{SI}$ is the corresponding fishing mortality rate.

For the embryonic stage, a mean natural mortality value (0.4 day$^{-1}$) was adopted, based on estimates by Somarakis et al. (2012). The natural mortality for early larvae is described as a function of egg abundance that was fitted to available field data (Somarakis and Nikolioudakis, 2007):

$$M_{SI} = -0.154 + 0.205 \cdot \log_{10}(\text{eggs/m}^2), \ \text{eggs/m}^2 > 22$$

where eggs is the number of eggs. A minimum value of 0.12 day$^{-1}$ was adopted based on the observed minimum larval mortality (see Fig. 9 in Somarakis and Nikolioudakis, 2007). A constant natural mortality rate (0.06 day$^{-1}$) was adopted for the late larval stage, following Mantzouni et al. (2007). Given the wide range and uncertainty of estimates on the juvenile mortality, the latter was treated as a calibrated parameter in order to achieve a better fit with field biomass estimates. Its value (4 year$^{-1}$) is within reported ranges (Mantzouni et al., 2007). Finally, fixed natural mortality rates were used for the adult age classes, as estimated for the stock assessment of anchovy in the NAS (Giannoulaki et al., 2014). All natural mortality values are listed in Table A.2.

Fishing mortality ($F_{SI}$) applied to the adult SIs, follows the separability assumption and is determined by the product of two components,

$$F_{SI} = F_{month} \cdot F_{position},$$

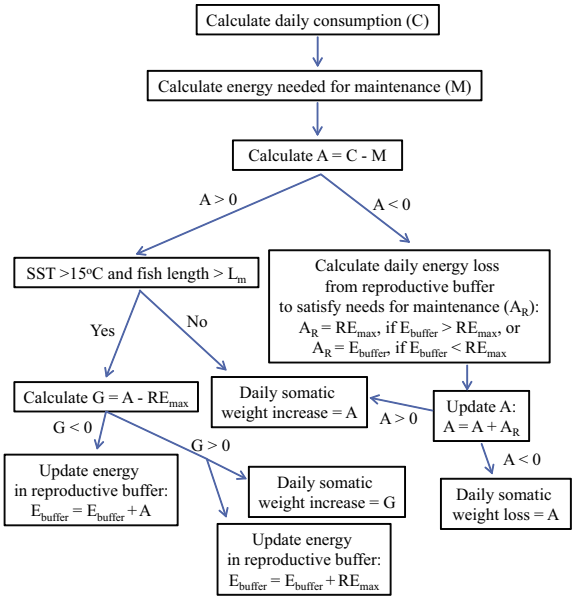


**Fig. 3.** Schematic illustration of the energy allocation algorithm. SST: Sea surface temperature. $L_m$: length at maturity for anchovy in the NAS (105 mm). $E_{buffer}$: energy in reproduction buffer. $RE_{max}$: fixed maximum energy amount that can be channelled daily from/to the reproductive buffer.

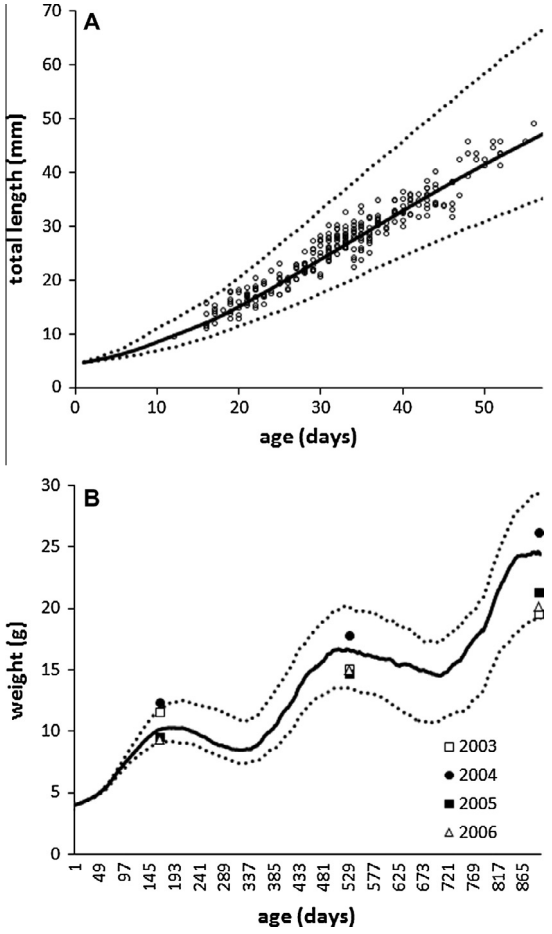


**Fig. 4.** (A) Mean individual growth trajectory (solid line) simulated by the model for anchovy larvae produced in June/July 2003–2006. Dotted lines: upper and lower (25% and 75%) quantiles. Data points represent length-at-age (number of otolith micro-increments) data from larvae collected in the NAS during July 2007 and July 2008 (Schismenou, 2012). (B) Mean individual growth trajectory (solid line) simulated by the model for anchovy adults (simulation starting on January 1st 2003). Dotted lines: upper and lower quantiles. Data points labeled with different symbols indicate mean weight of fish at age-1, age-2 and age-3 (otolith readings) from samples collected during the acoustic surveys of 2003–2006.

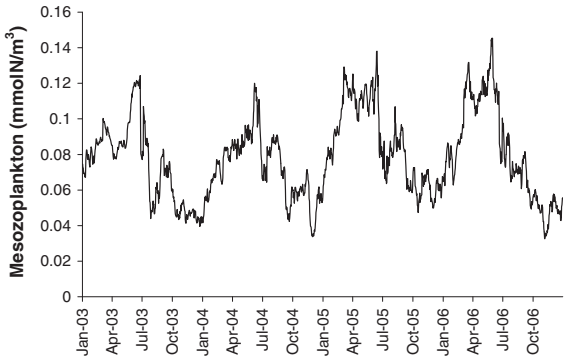


**Fig. 5.** Simulated mean mesozooplankton biomass at the juveniles/adults super-individuals location.

where $F_{month}$ is a monthly varying fishing mortality (year$^{-1}$) that describes the seasonality in the fishing effort and $F_{position}$ is a spatial index, which characterizes the fishing grounds. The values of $F_{month}$ (Table A.2) were derived from the monthly anchovy catches (estimated as a percentage of the annual catch, Fig. B.2), so that the mean $F_{month}$ equals the estimated annual fishing mortality

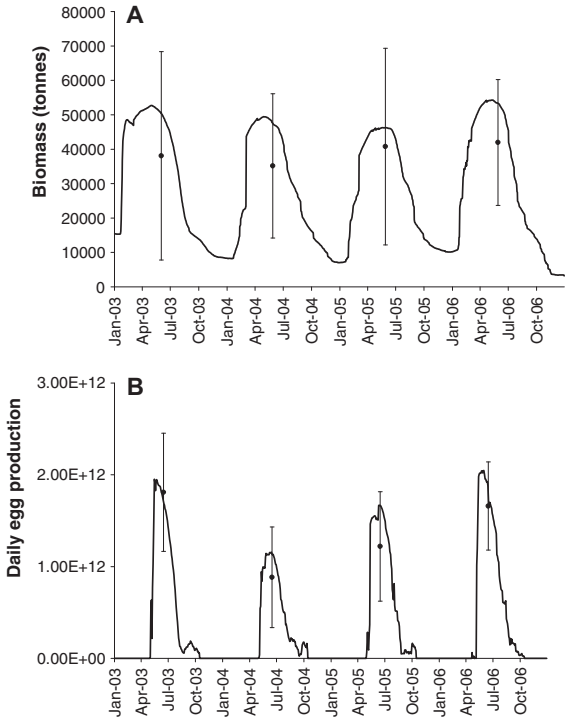


**Fig. 6.** (A) Model simulated anchovy biomass, (B) daily egg production (number of eggs produced daily by the fish population) from 2003 to 2006. Data points are respective estimates from the acoustic and daily egg production surveys of 2003–2006 (Somarakis et al., 2012) recalculated for the area covering the model domain. Error bars: approximate confidence intervals (±2SE).

(0.5 year$^{-1}$, Giannoulaki et al., 2014). $F_{position}$ takes the values 0 or 1, when the current position of the SI is found within or outside the identified fishing grounds, respectively. The fishing grounds of anchovy in the NAS include the continental shelf areas of the Thermaikos Gulf, the Thracian Sea and the Strymonikos Gulf (Fig. 1) as indicated by recent maps of the spatial distribution of fishing effort (Kavadas and Maina, 2012).

*Reproduction*

Fish reproduction has been modelled in several ways within a population fish model; either by using data fitted to spawner–recruit relationships (Megrey et al., 2007), either assuming that the total number of eggs produced is proportional to fish weight and temperature (Oguz et al., 2008) or by adopting a dynamic energy allocation algorithm, in which energy stored in a so called 'reproduction buffer' determines the number of egg produced under predefined spawning rules (Pecquerie et al., 2009). In the present study, the latter approach was followed, since it has the advantage of relating the spawning activity in terms of timing, duration and intensity to changing environmental conditions and the physiological status of the fish. New SIs (egg SIs) are being produced by adult SIs through spawning, based on a reproduction module that considers all basic characteristics of the anchovy reproduction strategy in the NAS.

NAS anchovy is characterized by an extended spawning period (mainly from May to September), while its daily specific fecundity is variable between years, areas and seasons, in response to changes in environmental and trophic regimes (Somarakis et al., 2004, 2012). Variability is egg production is mainly due to the spawning fraction parameter, i.e. the proportion of mature females spawning each night (Somarakis et al., 2012). However, actively spawning European anchovy has a specific spawning biorhythm of about 3 days (Schismenou et al., 2012; Uriarte et al., 2012).

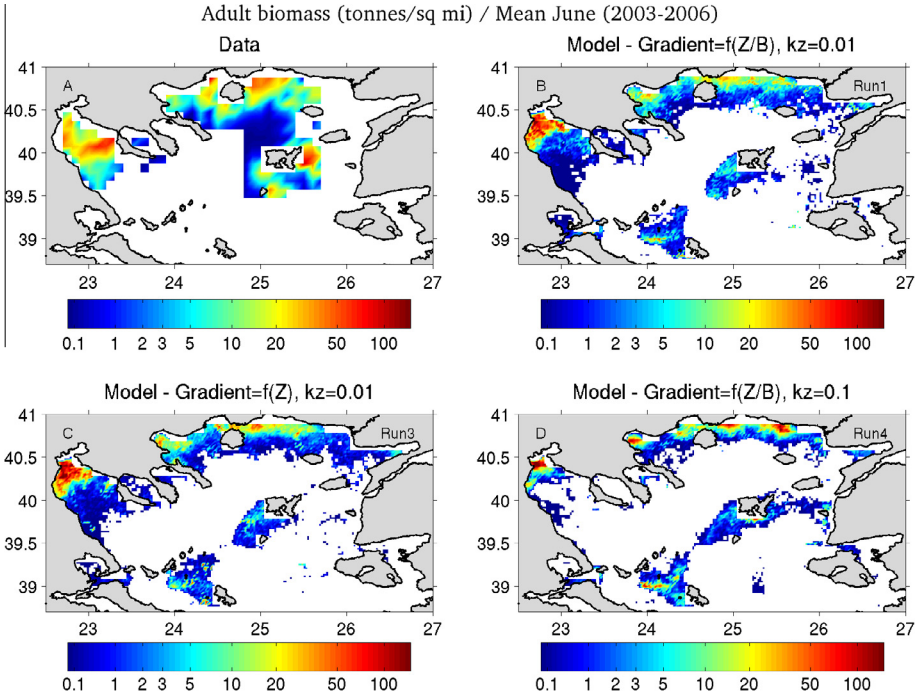


**Fig. 7.** Anchovy biomass (tonnes/square mile), (A) derived from acoustics and (B) model simulated, averaged over June 2003 to 2006, (C) same as B for the sensitivity simulation (Run3) employing the food gradient (instead of the food/capita gradient adopted in the reference simulation, Eq. (7)), (D) same as B but with $k_z = 0.1$ (Run4, $k_z = 0.01$ in the reference).

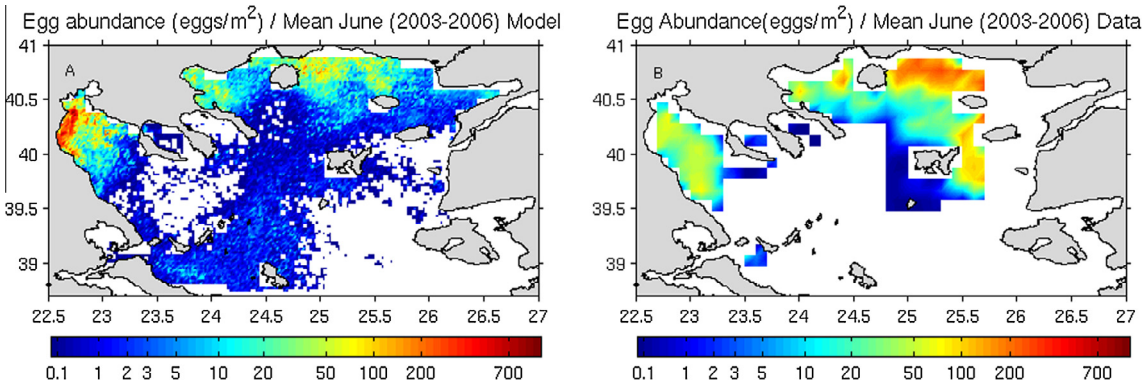


**Fig. 8.** (A) Model simulated and (B) DEPM derived egg abundance, averaged over June 2003 to 2006.

The NAS anchovy stock is also considered to be primarily an income breeder (Somarakis et al., 2004). It is therefore reasonable to consider that energy allocated to reproduction derives primarily from direct food intake. In that sense, the egg production module developed for anchovy in the present study is dynamic and is based on the bioenergetics equation. The main steps and assumptions in the development of the module were centred on a new conceptual model for anchovy vitellogenesis (Schismenou et al., 2012) and are described below:

(1) According to the findings of Hunter and Leong (1981) for the northern anchovy (*Engraulis mordax*) and Schismenou et al. (2012) for the Mediterranean anchovy (*E. encrasicolus*), recruitment of successive vitellogenic batches during the spawning period occurs in pulses and the number of vitellogenic oocytes in the ovaries of actively spawning fish equals two times the batch fecundity (number of eggs produced per spawning event). After their recruitment, the oocytes of a new vitellogenic batch grow continuously and need about two times the inter-spawning interval (number of days between two successive spawning events) to complete their development. The same time is approximately needed to resorb all vitellogenic oocytes of the ovary (i.e. two batches) through atresia in the absence of any food, as revealed from laboratory experiments (Hunter and Macewicz, 1985). Hence, the daily energy allocated to reproduction or from gonad to maintenance through atresia (in case of lack of food), can be considered as fixed (growth and atresia of vitellogenic oocytes are continuous processes) and equals to the energy contained in a spawning batch divided by the inter-spawning interval (1/S, where S is the spawning frequency). In population terms, this fixed energy amount equals to the product of individual egg energy and daily specific fecundity (DSF). DSF (Lasker, 1985) is the number of eggs produced daily per gram of population (in this case, super-individual).

(2) Assuming that the relative batch fecundity is 260 eggs per gram of females, the inter-spawning interval (spawning biorhythm) is 3 days (spawning fraction: 0.33), and the

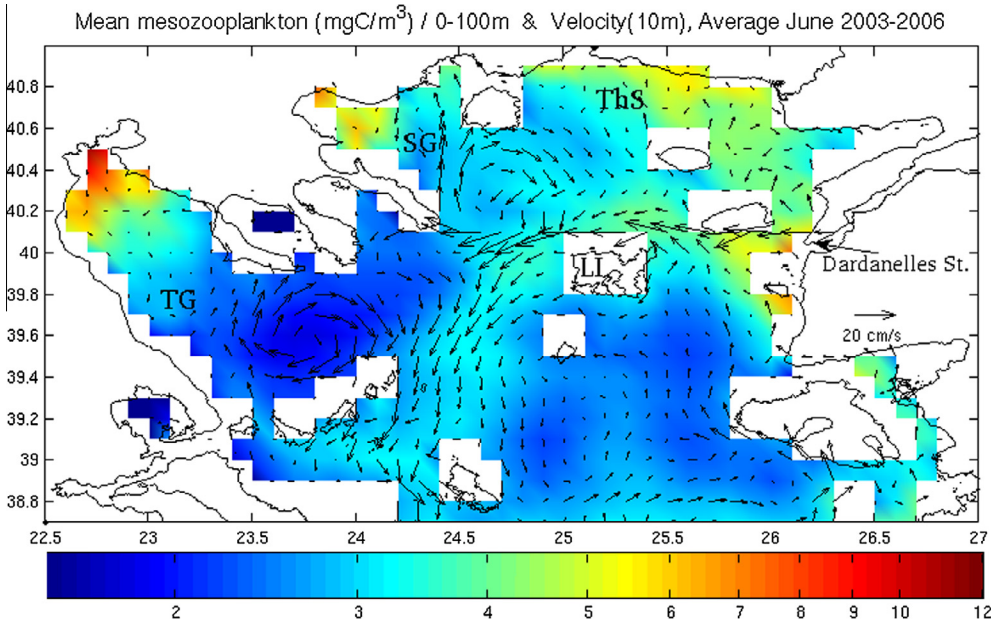


**Fig. 9.** Model simulated mean 0–100 m mesozooplankton biomass (mgC/m$^3$) and near surface velocity field, averaged over June 2003–2006. The Thracian Sea (ThS), Thermaikos gulf (TG), Strymonikos gulf (SG), Limnos Island (LI) and Dardanelles straits are indicated.

weight-specific sex ratio 0.54 (these are the average values observed for these parameters in the NAS during the Daily Egg Production surveys in June [Somarakis et al., 2012]), the daily specific fecundity is set at 46 eggs per gram of super-individual per day. This can be considered as the amount of energy that can be allocated daily to reproduction and accumulated in the 'reproductive buffer', (*sensu* Pecquerie et al. (2009)). Taking into account the energy of an egg, $CAL_{egg} = 5600$ J g egg$^{-1}$ (Valdés, 1993), the energy density coefficient for zooplankton $CAL_Z$ and the mean wet weight of an anchovy egg ($W_{egg} = 27.7$ μg, Politikos et al., 2011), the daily 'reproductive' energy is $RE_{\max} = 46 \cdot \frac{CAL_{egg} \cdot W_{egg}}{CAL_Z} = 0.0028$ g prey g fish$^{-1}$ day$^{-1}$. $RE_{\max}$ is actually the maximum amount of energy that can be channelled to/from the reproductive buffer.

(3) *Thresholds for reproduction.* In order to allocate energy to the reproductive buffer, the fish should be larger than 105 mm (length at first maturity in the Aegean Sea, Somarakis et al., 2006) and surface temperature >15 °C (Somarakis and Nikolioudakis, 2007).

(4) *Daily energy allocation algorithm* (Fig. 3). Energy from consumption is first channelled to all other functions except reproduction and growth. If fish length is >105 mm and sea surface temperature >15 °C, the remaining energy (A) goes to the reproductive buffer (first) and soma (secondly). If not, energy already in the reproductive buffer (first) and fish soma (secondly) goes to maintenance (to meet daily maintenance costs). If the daily energy is enough for maintenance and reproduction, the remaining goes to growth (increase in weight).

(5) *Production of egg super-individuals.* Every day, each adult SI can produce a new egg SI equal to 46 eggs per gram of adult SI, given that the amount of energy existing in its reproductive buffer suffices. The initial position of the egg SI is the position of the adult SI.

*Movement*

The fish SI trajectories are simulated in two dimensions, following the Lagrangian approach in continuous space (Watkins and Rose, 2013). The position of a SI ($x^{k+1}, y^{k+1}$) at time $k + 1$ is updated as:

$$\begin{aligned} x^{k+1} &= x^k + U \cdot \Delta t \\ y^{k+1} &= y^k + V \cdot \Delta t, \end{aligned} \tag{2}$$

where $U, V$ are the $x, y$ components of the fish velocity at time $k$ and $\Delta t$ is the time step (s). We should note that the SI location is transformed from the geographic coordinates (longitude, latitude) to Cartesian $(x,y)$, before the SI displacement is calculated in meters (Eq. (2)). Its new geographical location is then updated from the Cartesian coordinates taking into account the earth's curvature by using the following transformation:

$$dLon = \frac{dx}{dg \cdot cos(Lat)}, \quad dLat = \frac{dy}{dg} \tag{3}$$

where $(dLon, dLat)$ and $(dx, dy)$ are the displacements in geographical and Cartesian coordinates, $Lat$ is the latitude and dg is the conversion factor from degrees to meters (~111,300 m/degree).

Eggs and early larvae are treated as passive tracers, whose transport is heavily influenced by physics (Lett et al., 2009; Huret et al., 2010). For simplicity, the vertical movement that depends on their buoyancy is not considered in the present model and both eggs and early larvae are assumed to have a uniform vertical distribution in the 0–30 m layer (Allain et al., 2007). This assumption is supported by studies on the vertical distribution of these stages (Olivar et al., 2001; Sabatés et al., 2008). Thus, in the case of egg and early larval SI, the fish velocity is

$$\begin{aligned} U &= u_c + a \\ V &= v_c + a, \end{aligned} \tag{4}$$

where $u_c$, $v_c$, are the $x, y$ components of the local average current velocity (m/s) in the 0–30 m layer at the SI's location and $a$ is a uniform random number between −1 and 1, which is used to parameterize not included effects (e.g. turbidity).

In contrast to early life stages, the movement of late larvae, juveniles and adults is not dictated by the physics, since they have the ability to actively determine their displacement (Lett et al., 2009). The implemented movement module for these stages

simulates fish movement following conceptually the restricted-area approach (Tu et al., 2012; Xu et al., 2013).

In this case, the fish velocity is calculated from the sum of three components:

$$U = u_c + u_f + R_x$$
$$V = v_c + v_f + R_y, \quad (5)$$

where $(u_c, v_c)$ is the ocean current velocity, $(u_f, v_f)$ defines the fish swimming drift and $(R_x, R_y)$ denotes the random part of the movement.

Descriptively, fish are assumed to be able to evaluate the combined effects of environmental (available food, currents), bathymetric and population parameters in the surrounding cells and then direct their orientation to the optimal cell. The net swimming velocity of fish accounts also for the ocean current velocity in order to achieve the desired direction. In case that the magnitude of the current is greater than the fish maximum cruising speed, then no active swimming is applied and the fish is assumed to be advected by the current along with some random movement.

The fish swimming drift is given by:

$$u_f = (FiS - CS) \cdot \left(GF_x^n \cdot FV + GT_x^n \cdot FT\right)$$
$$v_f = (FiS - CS) \cdot \left(GF_y^n \cdot FV + GT_y^n \cdot FT\right). \quad (6)$$

$FiS = a_L \cdot L + R_L \cdot \varepsilon$ is the maximum sustainable fish swimming speed (m/s), which is described as a function of body length (L). FiS is perturbed by $R_L$, which represents the maximum degree of error, whereas $\varepsilon$ is a uniform random number between −1 and 1. The values of $a_L$ and $R_L$ are shown in Table A.2. *CS* is the magnitude of the ocean current, while $\left(GF_x^n, GF_y^n\right)$ and $\left(GT_x^n, GT_y^n\right)$ are normalized unit vectors pointing to the direction of high zooplankton densities and preferred water column depths, respectively. Furthermore, *FV* is a function of zooplankton biomass (see below) used to slow down the fish swimming speed, when there is enough food at its current location, while *FT* is a function of water column depth (see below) that relates fish movement to certain bathymetric ranges, known from the fish habitats. In case of FiS < CS, the fish drift becomes zero, i.e. $u_f = v_f = 0$ and individuals are assumed to be advected by the currents. The maximum fish swimming speed for adult fish (0.17–0.35 m/s) is generally higher than typical current speeds in the N. Aegean. Therefore, the above assumption is relevant mostly for early life stages (larvae, juveniles).

In order to prevent the overcrowding of the adult SIs in areas with high zooplankton biomass, density-dependent feeding was taken into consideration. Therefore, the food gradient is calculated based on the ratio of the zooplankton over the total fish biomass in surrounding cells. It is calculated as

$$GF_x = \frac{\partial\left(\frac{Z}{B}\right)}{\partial x}, \quad GF_y = \frac{\partial\left(\frac{Z}{B}\right)}{\partial y}, \quad (7)$$

where $Z$ and $B$ represent the available zooplankton biomass (calculated based on the assumed SI vertical distribution, see Section 'Coupling of LTL with the IBM model') and the total fish biomass respectively. Under this assumption, SIs will preferably move towards cells with maximum food per capita availability, avoiding "overcrowded" grid cells, where food per capita is decreased, despite their high zooplankton availability. The food per capita ($Z/B$) based gradient is used, provided that anchovies are not found under unfavourable conditions, experiencing a weight loss. If this is the case, then a simple food gradient (replacing $Z/B$ with $Z$ in Eq. (7)) is used, assuming that the fish will move towards maximum food (regardless of the presence of other SIs), in order to avoid starvation. The food gradient vector is normalized to a unit vector $\left(GF_x^n, GF_y^n\right)$ by dividing with its magnitude, $\left(GM = \sqrt{(GF_x)^2 + (GF_y)^2}\right)$.

The role of the function *FV* is to introduce a mechanism that will slow down the direct movement of the fish towards higher prey concentration cells, when there are adequate food resources at its present location, allowing the fish to remain in a favourable location. The function *FV* has the form $FV = 1 - \frac{Z_{SI}}{Z_{SI} + k_Z}$, where $Z_{SI}$ is the interpolated zooplankton biomass (see next Section 'Coupling of LTL with the IBM model') at the SI's location and $k_Z$ is a "half-saturation" calibrated parameter, representing the zooplankton concentration, where *FV* is reduced to half. For $Z_{SI} \gg k_Z$, *FV* will approach zero.

The bathymetry gradient is calculated as:

$$GT_x = \frac{\partial h}{\partial x}, \quad GT_y = \frac{\partial h}{\partial y}, \quad (8)$$

where $h$ is the depth of the water column. As above, the gradient vector is normalized to a unit vector $\left(GT_x^n, GT_y^n\right)$ by dividing with its magnitude.

The function *FT* (Eq. (9)) was introduced as a mechanism to keep juvenile and adult SIs from moving towards very deep waters (>300 m) or near the coastline. This parameterization was based on existing knowledge on the NAS anchovy habitats (Giannoulaki et al., 2008, 2013). In case of deep waters ($D_{wc} > 300$ m), *FT* approaches −1 and the topography gradient term in Eq. (6) acts to direct the fish towards shallower waters (a positive gradient is directed to higher values). Similarly, when SIs move near the coastline, the function results in a movement to the opposite direction, towards offshore waters. It should be noted that the effect of bathymetry on the fish movement is only activated, through the *FT* function, when the water column depth in the SI location gets higher than a maximum depth (300 m) or if the SI is moving towards the coastline. Otherwise, the FT function is zero (Eq. (9)) and anchovy SIs are moving based only on the food gradient. The above information is summarized as follows:

$$FT = \begin{cases} -\frac{D_{wc}}{D_{wc} + d_{wc}}, & D_{wc} > 300m \\ 1 - \frac{D_{wc}}{D_{wc} + d_{wc}}, & D_{wc}\ \text{coastline} \\ 0, & \text{otherwise} \end{cases} \quad (9)$$

where $D_{wc}$ is the interpolated depth of the water column at the current location of the SI and $d_{wc}$ is a depth parameter that controls the steepness of the function. The parameter values of the movement module are listed in Table A.3.

The random components of movement are calculated by

$$R_x \text{ and } R_y = \sqrt{\frac{6 \cdot dif}{\Delta t}} \cdot \varepsilon, \quad (10)$$

where *dif* is the horizontal diffusivity at the SI location (calculated by the hydrodynamic model following a Smagorinsky formulation, (Smagorinsky, 1985)) and $\varepsilon$ a uniform random number between −1 and 1.

### *Coupling of LTL with the IBM model*

The anchovy IBM is on-line coupled to the LTL model. The outputs from the hydrodynamic (currents, temperature, horizontal diffusion) and biogeochemical (zooplankton biomass) models are provided as inputs to the IBM, describing the three-dimensional environment of the fish. In particular, zooplankton biomass from different groups (microzooplankton, mesozooplankton) is used as a food source by anchovy (Fig. 2), with a different preference, depending on the fish life stage as shown in Table A.1.

Furthermore, the anchovy IBM and LTL models are two-way, dynamically coupled. Thus, the heterotrophic plankton biomass (microzooplankton, mesozooplankton) that is consumed by the fish is removed in the biogeochemical model, (as additional predation mortality exerted by the fish). At the same time, fish energy losses that are calculated by the bioenergetics model are fed back to the LTL model. In particular, fluxes due to the fish egestion and specific dynamic action are directed to the organic particulate (detritus) matter pool (POC, PON, POP) of the LTL, while fluxes due to excretion are returned as phosphate and ammonia.

Within each SI of the fish population, a vertical distribution in the water column at the SI location is assumed, based on the distribution of the available food (zooplankton concentration). The calculated distribution $F(j,z)$, which is a function of fish life stage $j$ and depth $z$, is maximised around maximum food availability and it is based on its zooplankton prey preferences:

$$F(j,z) = \frac{food(j,z)^2}{food(j,z)^2 + k_f(j,food)}$$

where $food(j,z) = pref_4(j) * Z4(z) + pref_5(j) * Z5(z)$ is the total available prey at depth $z$ for life stage $j$ over the zooplankton groups (mesozooplankton $Z4(z)$, microzooplankton $Z5(z)$) with the corresponding feeding preferences $pref_4(j)$ and $pref_5(j)$. Finally, $k_f(j,food)$ is a parameter, which controls the steepness of the distribution function. The above sigmoid function is normalised to 1.

Late larvae, juvenile and adult anchovies are assumed to perform diurnal vertical migrations, staying below the thermocline (>30 m) during daytime and in the upper water column layer during the night (0–30 m). Thus, the assumed distribution $F(j,z)$ is calculated within the 0–30 m layer or below that, depending on the time of the day.

The vertical distribution of zooplankton is first calculated in the SI surrounding grid points of the LTL grid and is then bi-linearly interpolated at the SI location. The opposite procedure is followed in the calculation of the returned fluxes to the LTL model; they are distributed to the 4 surrounding points. Thus, using the distribution function that represents the fish vertical distribution at the SI location, the fluxes in terms of zooplankton consumption, as well as of the released inorganic nutrients and organic matter are calculated at each depth of the water column and applied to the surrounding LTL model grid points. The fish return fluxes for each depth $z$ are calculated as:

$$Flux(j,z) = Flux_{Fish} \cdot F(j,z),$$

where $Flux_{Fish}$ is the total flux from the fish SI in terms of consumed zooplankton or released inorganic nutrients/organic matter and $F(j,z)$ is the distribution function. In this way, the fish zooplankton consumption and released by-products are distributed analogously in the water column of the LTL model at the same time step, based on the assumed vertical distribution of the fish. Given the different units of the fish (g wet weight) and the LTL (mgC/m$^3$, mmol N, P/m$^3$) models, the fish biomass (*f_biom*) is translated to carbon (*fc_biom*), nitrogen (*fn_biom*) and phosphorus (*fp_biom*) average (a different weight is applied on the flux of each depth, based on the vertical distribution $F(j,z)$) concentrations in the water column of the LTL grid cell, where the fluxes are applied:

$$fc\_biom(\mathrm{mgC/m^3}) = f\_biom(\mathrm{g\ ww}) * ffc(\mathrm{mgC/g\ ww})/vol(\mathrm{m^3}),$$

$$fn\_biom(\mathrm{mmol\ N/m^3}) = qnF(\mathrm{mmol\ N/mgC}) * fc\_biom(\mathrm{mgC/m^3}),$$

$$fp\_biom(\mathrm{mmolP/m^3}) = qpF(\mathrm{mmolP/mgC}) * fc\_biom(\mathrm{mgC/m^3}),$$

where *ffc* is a conversion factor from fish gram ww to mgC, based on the carbon content of anchovy dry weight (Czamanski et al., 2011), assuming that dry weight is 32% of wet weight (Tudela and Palomera, 1999), $(qnF, qpF)$ is the assumed ratio of the nitrogen and phosphorus over carbon pools in the fish biomass (Czamanski et al., 2011) and *vol* is the water column volume at the LTL grid cell $(dx * dy * depth)$, where the fluxes are applied.

The returned fluxes are then calculated as:

$$Flux_{carbon}(Z4,Z5) = fc\_biom * CON(Z4,Z5),$$

$$Flux_{nitrogen}(Z4,Z5) = fc\_biom * CON(Z4,Z5) * qnZ4,5,$$

$$Flux_{phosphorus}(Z4,Z5) = fc\_biom * CON(Z4,Z5) * qpZ4,5,$$

$$Flux(ammonia, phosphate) = fn,p\_biom * EX,$$

$$Flux(POC,N,P) = fc,n,p\_biom * (EG + SDA),$$

where *Z4*, *Z5* are the mesozooplankton and microzooplankton LTL groups respectively and $CON(Z4,Z5)$, *EX*, *EG* and *SDA* are respectively the consumption (on *Z4*,*Z5*), excretion, egestion and dynamic action rates (day$^{-1}$) calculated by the fish bioenergetic model. Since the fish biomass has different C:N:P internal quotas $(qnF, qpF)$ from the consumed zooplankton $(qnZ4,5, qpZ4,5)$, the excess carbon, nitrogen or phosphorus is assumed to be excreted as dissolved organic matter following Broekhuizen et al. (1995), so that the fish can maintain a constant C:N:P internal quota. The related parameter values are shown in Table A.4.

### *Simulation setup*

A hindcast inter-annual simulation of the model for 2003–2006 period was performed, to validate the full life cycle model against data derived from field observations and assess its skill in reproducing the principal characteristics of the fish population variability in the NAS.

#### *LTL initialisation/forcing*

The atmospheric forcing for the inter-annual 2003–2006 simulation was obtained from the POSEIDON operational forecast (www.poseidon.hcmr.gr; Papadopoulos et al., 2002). The water discharge for major NAS rivers was set to climatological mean values, while river nutrient concentrations were based on average yearly mean in situ data for the 1995–2000 period (Skoulikidis, 2009), in the absence of monitoring data for the 2003–2006 period. The Dardanelles water exchange is parameterized through a two-layer open boundary condition (Nittis et al., 2006) with prescribed water inflow/outflow and salinity, adopting climatological biogeochemical (inorganic nutrients and non-living organic matter) data averages (Tugrul et al., 2002; Polat et al., 1998). The initial fields for dissolved inorganic nutrients were obtained from the Medatlas 2002 climatology (http://www.ifremer.fr/medar/) and the coupled model was spun-up for 3 years (2000–2002).

#### *IBM initialization*

The full life cycle model was initialized on 1st January 2003. Acoustic survey data were available for June 2003–2006. However, given the unknown magnitude of the larval abundance, it was found preferable to initialize the model in the winter period, when early life stages are not present (summer is the spawning period). Thus, using the estimated numbers-at-age from the acoustic survey of June 2003, the respective numbers for juvenile/adult anchovy at the 1st January were back-calculated, after accounting for natural and fishing mortalities between January and June. The estimated numbers-at-age on 1st January were assigned to 1000 super-individuals per year class. It was assumed that three year classes were present in January with respective ages: age-0: 0.5, years, age-1: 1.5 years, and age-2: 2.5 years. The length–weight

relationship (Section 'Bioenergetics') and a generic von Bertalanffy growth equation for the NAS anchovy stock (Machias et al., 2000) were used to calculate the respective length and weight at age on January 1st.

The initial positions of the super-individuals on 1st January 2003 were defined based on published statistical habitat models of anchovy in the NAS during winter (Giannoulaki et al., 2013). Using these models, the points of the LTL model grid that had a higher than 50% probability for anchovy presence were defined. The SIs were then randomly spread around each of these points, within a radius of 10 km.

For computational efficiency, a maximum number of 15,000 SIs was chosen. This was allocated to 6000 SIs for eggs, 4000 for larvae, 2000 for juveniles and 1000 SIs for each of the three adult age classes. When the maximum number for a life stage is exceeded, random pairs of SIs (of this same stage/age class) that are found within a certain distance (~10 km) are merged. The attributes of the new merged SI are either weighted averaged (weight, length, position, reproductive energy) or summed (population number). In this way, the number of SIs, which would otherwise increase from year to year, is kept within reasonable limits.

*Model validation*

The simulated fish somatic growth, spatial distribution of biomass, and egg abundance, total anchovy biomass and egg production over the 2003–2006 period were compared against data derived from field observations for the same 2003–2006 period in June (Somarakis et al., 2012; Giannoulaki et al., 2014). The estimates of total egg production and acoustic biomass published in Somarakis et al. (2012) were recalculated to include the model domain only, i.e. excluding the highly enclosed North Evoikos Gulf. Additionally, for larval growth, data on length-at-age from specimens collected at a coastal site of the NAS (Schismenou, 2012) were used.

*Sensitivity runs*

A series of sensitivity simulations were performed to investigate the effect of different formulations adopted for key processes, such as reproduction and movement. In particular, a simulation adopting a constant fecundity (Run2) was compared to the reference simulation (Run1), in order to examine the effect of the dynamic egg production. With regard to fish movement, two additional simulations were performed. In the first (Run3), a simple food ($Z$) rather than the food per capita ($Z/B$) based gradient (Eq. (7)) was used to direct fish movement. In the second (Run4), a higher value was used for parameter $k_Z$ that controls the amount of prey, at which the fish slow down in order to maintain position in a favourable area. Finally, in order to investigate the effect of the anchovy population on plankton through the two-way (IBM–LTL) coupling, the reference simulation was compared with a simulation of the LTL not coupled to the IBM (Run5) and one that adopted a two-way coupling for consumed zooplankton but not for returned fish by-products (Run6). The attributes of the different sensitivity simulations are shown in Table 2.

## Results

As already mentioned, the lower trophic level ecosystem model implemented here is an existing model already applied, validated and analyzed in the NAS ecosystem (Tsiaras et al., 2012, 2014). Thus, in this paper, we focus mainly on the fish dynamics and the fish effect on LTL model plankton dynamics through the coupling process.

*Growth*

The fish model simulated well the growth of larvae, as shown by the comparison with the available field data (Fig. 4A). The average individual growth trajectory for larvae simulated by the model during June–July fitted well the length-at-age data of larvae captured in July.

Furthermore, growth in terms of weight of juveniles/adults was also well reproduced by the full life cycle model (Fig. 4B). The model simulated weights matched well the observed average weights-at-age of fish aged 1, 2 and 3 years from the acoustic surveys in June. A prominent characteristic of the growth curve is that the simulated growth follows the seasonal variations of its main prey, i.e. the mesozooplankton biomass, which increases significantly till early summer and decreases gradually from late summer till the end of January (Fig. 5). Overall, the seasonal variability of zooplankton follows the variability of primary production and phytoplankton biomass (not shown), with a time-lag of one month, showing maximum concentrations during the spring period (April–June). The seasonality of the plankton productivity is related to the entrainment of subsurface nutrients triggered by increased vertical mixing during winter, as well as the seasonal variability of river and Black Sea Water (BSW) nutrient inputs that peak during the same period (Tsiaras et al., 2014, see also later discussion on Figs. 7 and 9).

*Biomass*

The modelled anchovy biomass (juveniles and adults) from 2003 to 2006 is illustrated in Fig. 6A. Model results were in agreement with biomass estimates from the acoustic surveys in June, indicating that the full life cycle model efficiently reproduces the magnitude of the anchovy biomass in the study area. It should be noticed that biomass estimates from acoustics are characterized by low precision; the biomass of the NAS anchovy stock is also underestimated by acoustics because the surveys do not cover the easternmost part of the Aegean Sea (the Turkish territorial waters). One of the prominent characteristics in the model simulation is the biomass increase in spring. During this period, anchovies are able to increase their weight by preying on the abundant zooplankton stocks (Fig. 5). Following this growth period, the increase of fishing mortality combined with the gradual decrease of prey availability and the energetic cost of spawning result in the decrease of adult biomass after July. From October to January, the decrease of biomass continues mainly due to increased starvation mortality of juveniles/adults.

*Egg production*

At the population level, the simulated spawning period, as well as the magnitude of the peak egg production was in agreement with the existing knowledge on the anchovy spawning seasons (spring to autumn, Somarakis et al., 2004, 2006) and the daily egg production estimates from the DEPM surveys in June (Fig. 6B), respectively. Field egg production estimates are highly uncertain and do not include the eggs produced in Turkish territorial waters (Somarakis et al., 2012). However, the inter-annual variations in peak egg production were similar between the model simulation and field estimates. Model results also indicate that spawning starts in late April, with a peak in late May–early June. Seasonal changes in the simulated egg production were very similar among different years. A sharp increase in egg production is observed at the beginning of the spawning season, which is due to the temperature threshold of the egg production module (15 °C), combined with the high zooplankton concentrations during that period (Fig. 5). After peak spawning, the simulated

**Table 2**
Sensitivity simulations attributes.

| | Difference from Reference | Reference (Run1) |
|---|---|---|
| Run2 | Constant egg production | Dynamic egg production |
| Run3 | Food gradient = $f(Z)$ | Food gradient = $f(Z/B)$ |
| Run4 | $Kz = 0.1$ | $Kz = 0.01$ |
| Run5 | Not coupled (only LTL) | Two-way coupled (zooplankton + fish by-products) |
| Run6 | Two-way coupled (zooplankton) | Two-way coupled (zooplankton + fish by-products) |

egg production decreases steadily from June to September, to practically cease in October. This decrease in egg production matches closely the decrease in mesozooplankton availability (Fig. 5). The 'tail' of the egg production curve in October is due to few SIs occurring within zooplankton-rich spots that can still acquire enough energy for reproduction.

*Spatial distribution of anchovy biomass and egg abundance*

In Figs. 7 and 8, the simulated average spatial distributions of anchovy biomass and egg abundance for the June 2003–2006 period are shown against contour maps of acoustic anchovy biomass and egg abundance from DEPM, again averaged for the June 2003–2006 period and linearly interpolated on the LTL model grid.

The simulated distribution of anchovy biomass (Fig. 7B) is characterized by increased aggregations in three subareas: (a) the Thermaikos Gulf (TG), (b) the enclosed area of Strymonikos Gulf (SG) and (c) along the continental shelf of the Thracian Sea (ThS) (see Figs. 1 and 8). In situ data show a similar pattern, although with slightly higher biomass levels in the eastern part of NAS (Fig. 7A), particularly at the east and south of the Limnos Island (LI). The increased anchovy biomass in the latter area is related to the Black Sea Waters (BSW) discharge from the Dardanelles straits that contribute to local enrichment, triggering an increased primary and secondary production (Siokou-Frangou et al., 2002). As shown in Fig. 8, the LTL model reproduces increased mesozooplankton biomass along the pathway of BSW that is however mainly simulated in the north of Limnos Island. A slightly different BSW pathway, with a more enhanced southern branch has indeed been simulated during summer period with a hydrodynamic model of finer resolution (unpublished data). This possible miss-representation of the BSW pathway with the relatively coarse hydrodynamic model used here, might partially explain the deviation between the model simulated and field observed anchovy distribution.

A prominent characteristic of oligotrophic systems is the tight coupling of the various components in the food chain, exhibiting a co-variation both in space and time with a time lag according to their specific growth time scales. As shown in Fig. 7 and 8 the areas supporting high fish biomass are those where maximum stocks of zooplankton are simulated. Higher concentrations for zooplankton are generally found in three subareas: the northern part of TG, the inner part of SG and the coastal waters of the ThS. The key characteristics contributing to this are: the shallow depth, which creates a strong coupling between the pelagic and benthic systems enhancing remineralisation and the return of nutrients; and the source of nutrient inputs such as rivers, or the Black Sea Waters (BSW). Especially, TG accepts significant riverine loads and more particularly is a semi-enclosed area with relatively shallow waters, retaining nutrients and organic matter, in contrast to the eastern NAS areas, such as the Thracian Sea, where phytoplankton and zooplankton biomass are more strongly advected offshore (Tsiaras et al., 2014). The increased anchovy biomass that is simulated in Thermaikos gulf (Fig. 7B–D) is due to the relatively higher mesozooplankton biomass.

As compared to the field data, the model simulates a slightly higher egg abundance in Thermaikos Gulf and lower in the Thracian Sea and east of the Limnos Island (LI) (Fig. 9), showing however a similar pattern, with the same three sub areas of higher concentrations, as in the case of adult biomass (Fig. 7). These three areas constitute the major spawning and feeding grounds of anchovy in the NAS (Somarakis et al., 2012). The main difference in the horizontal distribution of egg abundance between model and field observations is found in the eastern part of LI, an area under the direct influence of BSW, where the model is not reproducing the observed high abundance of eggs. This was expected, since the model did not reproduce satisfactorily the observed adult concentration in this area (Fig. 7) as discussed above.

Taylor diagrams (Taylor, 2001) shown in Fig. 10, were used to graphically summarize the model skill in reproducing the spatial distribution of the observed fish biomass and egg abundance (Figs. 7A and 9B) derived from the survey data (average data over the June 2003–2006 period). We should note that the RMS error and standard deviation (STD) have been normalised to the data STD, while log-transformation has been applied on both the simulated and observed distributions before calculating the statistics. The simulated anchovy biomass (Adu1) presented a significant correlation (0.34) with the data (Figs. 7 and 10). It also exhibited similar variability, as the simulated STD was very close (0.95) to the data, while the RMS error was ~1.15. In the case of the egg abundance distribution (Egg1, Figs. 8 and 10), a slightly higher correlation coefficient (0.53) and a lower (0.9) RMS error were found, while the simulated STD was again close (0.85) to the data. The model showed a slightly better overall skill in the simulation of the egg abundance variability than that of biomass.

*Sensitivity results*

*Dynamic egg production*

In order to examine the effect of the dynamic egg production formulation, an additional simulation (Run2) was performed,

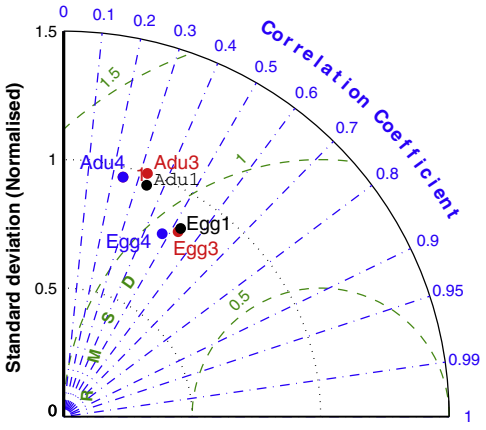


**Fig. 10.** Taylor diagram for the model simulated adult biomass (Adu) and egg abundance (Egg) against in situ data, averaged over June 2003–2006. The black dots (Adu1, Egg1) refer to the reference simulation (Run1), while the red (Adu3, Egg3) and blue (Adu4, Egg4) dots refer to the sensitivity simulations employing the food gradient (Run3, instead of the food/capita gradient Eq. (7)) and a higher $k_z = 0.1$ (Run4, $k_z = 0.01$ in the reference) respectively. Note that the model root-mean-square deviation (RMSD) and standard deviation (STD) have been normalised, by dividing with the data STD. The model skill may be evaluated by the dots location with regard to the lines representing the RMSD (circles starting from the *X*-axis), the STD (circles starting from the centre of the axis, STD = 1 means that the model has the same variability with the data) and the correlation coefficient (straight lines). (For interpretation of the references to colour in this figure legend, the reader is referred to the web version of this article.)

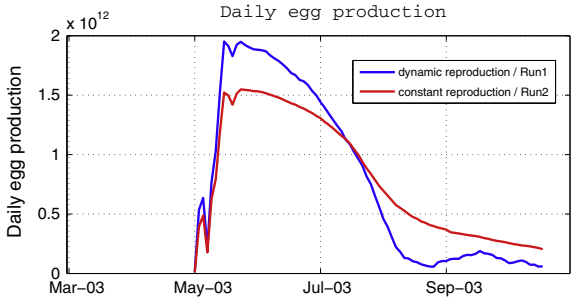


**Fig. 11.** Daily egg production simulated with the dynamic egg production module in the reference simulation (Run1, blue line) and with constant egg production (Run2, red line). (For interpretation of the references to colour in this figure legend, the reader is referred to the web version of this article.)

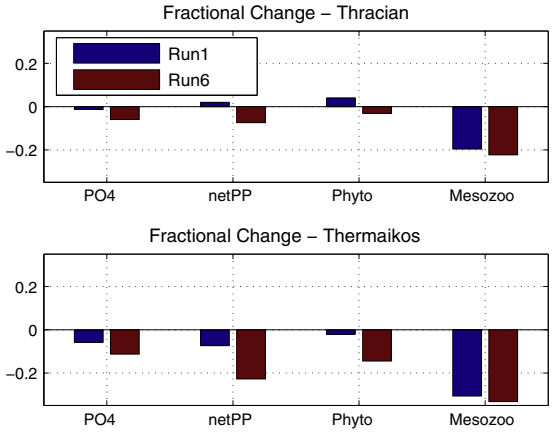


**Fig. 12.** Fractional change of the simulated Phosphate, Net Primary Production, Phytoplankton and Mesozooplankton biomass for Thracian Sea (top) and Thermaikos Gulf (bottom) with the reference simulation (Run1), where a two-way coupling of the IBM and LTL models is employed (both for zooplankton and fish by-products) and Run6 simulation, where fish by-products are not returned to the LTL model, compared to Run5 uncoupled LTL simulation. See Table 2 for simulations attributes.

adopting a constant daily specific fecundity. The latter was set equal to the 1st year's average fecundity, as derived from the dynamic module, which was about 75% of the maximum fecundity ($0.75 * 46$ eggs $g^{-1}$ $day^{-1}$). Thus, in the simulation with constant fecundity, the amount of spawned eggs depends only on the adult anchovy population biomass (egg production = $0.75 * 46$ eggs $g^{-1}$ - $day^{-1} *$ total biomass g). In Fig. 11, the effect of the dynamic reproduction formulation is illustrated. By comparing the reference simulation (blue line) with the one adopting a constant fecundity (red line), one can see that egg production in the latter case follows a similar seasonal pattern in terms of starting and ending time, showing also a peak during June, since the temperature and length thresholds for reproduction remain the same. However, it is noticed that the shape of the egg production curve is more spread within the spawning period, as compared to the dynamic reproduction module, since available energy for reproduction is not taken into account. So, even though fish weight starts to decrease from late summer (Fig. 4), SIs continue to actively produce eggs. As a result, egg production is higher in early autumn compared to the dynamic case, in which egg production practically ceases in autumn.

*Movement*

In order to investigate the effect of the adopted parameterization for fish movement, two additional simulations were performed. In the first (Run3), the food gradient was calculated based on the zooplankton field and not on its ratio on fish biomass (food per capita) (Eq. (7)) that was used in the reference (Run1) simulation, in order to prevent the overcrowding of SIs in areas with high zooplankton availability. The second sensitivity simulation (Run4) was identical to the reference, except that a higher value was used for the parameter $k_z$ (=0.1 mmol N/m$^3$), as compared to the reference ($k_z$ = 0.01 mmol N/m$^3$). As explained above (Section 'Movement'), the half-saturation constant $k_z$ represents an adequate prey concentration at which the fish slow down their movement, in order to remain in a favourable location. Thus, using a higher $k_z$ value would result in a more active movement towards areas with higher food resources. The attributes of different sensitivity simulations are presented in Table 2.

As shown in Fig. 7, the adult anchovy distribution from Run3 was very similar to the reference (Run1), except for a few patches of higher fish aggregation in Thermaikos Gulf and Thracian Sea. In Run4, differences were more pronounced, with fish distribution being characterized by stronger aggregations in the more productive coastal areas (inner Thermaikos gulf, Strymonikos gulf, Nestos and Evros River plume areas, indicated in Fig. 1). The distribution of fish in Run4 appears less realistic when compared to Run1 and Run3. This is also revealed by the Taylor diagrams (Fig. 10), comparing the simulated distributions against data from the acoustic surveys, in which Run4 presented a lower correlation ($r$ = 0.23) and a slightly higher RMS error, as compared to Run1 ($r$ = 0.34) and Run3 that exhibited similar skills.

*Link between LTL and IBM model*

To explore the effect of anchovy on the LTL model plankton dynamics, two additional simulations were performed. The first (Run5) was a simulation of the LTL model alone, not coupled to the IBM. In the second (Run6), the plankton biomass (microzooplankton, mesozooplankton) consumed by the fish was removed in the LTL (as additional, fish-induced predation mortality), but fish by-products (dissolved inorganic nutrients, organic matter) were not returned to the LTL, as in the reference (Run1) simulation (see Section 'Coupling of LTL with the IBM model' and Table 2 for simulations attributes). It should be noted here that in the coupled IBM–LTL model in which there is direct predation on zooplankton by the fish, a lower quadratic mortality (about −35% on average) for mesozooplankton (representing a top-predator closure term in the LTL, Edwards and Yool, 2000) was adopted, as compared to Tsiaras et al. (2014), in order to get similar results with previously validated zooplankton. The same (reduced) mortality was adopted in the other two (Run5, Run6) simulations in order to examine the overall effect of fish foraging on the plankton.

In the synoptic Fig. 12, some fractional changes in the two-way 'coupled' simulations Run1 and Run6 with regard to the 'uncoupled' Run5 are shown. In the Thracian Sea, a decrease of zooplankton biomass is simulated in both Run1 and Run6 due to the removal of zooplankton by fish. In contrast, the effect on phytoplankton is positive in Run1, due to the removal of predators and the supply of nutrients from fish by-products. Under Run6 scenario, zooplankton is further decreased relatively to Run1, as the nutrient shortage from the lost by-products results in the decrease of the phytoplankton biomass (the prey is reduced). Likewise, marked differences between the two scenarios were also simulated for the primary production rate, showing a significant decrease in scenario Run6, unlike Run1. In terms of phosphate there was a decrease under both scenarios although Run6 resulted in a higher reduction as expected.

A slightly different picture was obtained for the Thermaikos Gulf, where all variables were reduced under both scenarios and at much lower levels compared to the Thracian Sea. The reason was that the more abundant fish stocks in the Thermaikos Gulf

exerted a greater top down control on zooplankton. It is interesting to note that the removal of fish by products from the system did not have a significant effect on zooplankton unlike the primary producers and the nutrients stocks.

## Discussion

### Growth

The general growth pattern of the SIs was the result of seasonality in the zooplankton availability and the energetic cost of reproductive activity of adult fish. Slow growth rates from middle June to September and a somatic weight decrease (~12%) during autumn/winter was the main characteristic of anchovy growth simulated by the bioenergetics model. On the other hand, the increased zooplankton levels from May to July in the NAS, which coincide with the peak of the anchovy spawning period, were adequate to support the energy demands for egg production. The latter is of particular importance since anchovy is primarily an income breeder (Somarakis et al., 2004; McBride et al., 2014). In other bioenergetics studies investigating the impact of environmental variability on fish growth, the predicted growth in weight also showed seasonal changes, controlled by levels of food and temperature conditions (e.g. in Pacific herring (Megrey et al., 2007), anchovy in the Black Sea (Oguz et al., 2008), Bay of Biscay (Pecquerie et al., 2009), Gulf of Lion (Pethybridge et al., 2013) and the Yellow Sea ecosystem (Wang et al., 2013)).

### Reproduction

Spawning is a key module in the development of full life cycle fish models. Spawning locations and timing are critical for larval survival and subsequent recruitment success (Huse and Ellingen, 2008; Pecquerie et al., 2009). One of the main upgrades of our 3-D version of the anchovy bioenergetics model, compared to the 1-D model published in Politikos et al. (2011), was the inclusion of a dynamic reproductive module. Following the approach of Pecquerie et al. (2009), we used temperature and fish length thresholds to define the initialization/end of the spawning season, whereas the amount of energy stored in the 'reproduction buffer' determined the amount of eggs produced in subsequent spawning events. According to the simulations, spawning peaked at around June, whereas a high proportion of egg abundance were noticed over the continental shelf (Fig. 8A), mainly in areas with high prey densities (Fig. 9), implying the importance of adult feeding conditions in the production of eggs. Overall, the reproductive module was shown to work well, being in good agreement with existing biological knowledge on anchovy spawning season, location of spawning grounds in the NAS and the magnitude of population egg production during peak spawning. It should be noticed here that although the energy allocation algorithm developed here (Fig. 3) is suitable for income breeders, i.e., energy is only allocated to the reproduction buffer during the spawning season, it can be easily extended to include species that are primarily capital breeders, like the European sardine *Sardina pilchardus* (McBride et al., 2014), e.g. by simply allowing energy to be allocated to the reproduction buffer both in and outside the respective spawning season of the species.

Our reproduction module uses the daily specific fecundity parameter (DSF) which is a population reproductive parameter (it accounts for both females and males), i.e. it is appropriate for the super-individual approach. The daily specific fecundity is a function of sex ratio ($R$), spawning frequency ($S$) and relative batch fecundity ($F/W$) the values of which were fixed to the average values estimated in the field from a series of daily egg production method (DEPM) applications to the NAS anchovy stock (Somarakis et al., 2012). The weight-specific sex ratio and relative batch fecundity present low variability in the NAS (coefficient of variation for both parameters, CV = 0.12 (Somarakis et al., 2012)), but spawning frequency varies a lot (CV = 0.29). However, because the focus of DEPM surveys is on stock assessment, the existing spawning fraction estimates include in the denominator (of $S$) both the spawning capable (actively spawning) but also the maturing and post-spawning adult fish. Thus, the spawning fraction from DEPM surveys is not appropriate to calculate the 'true' spawning frequency and is highly variable. In recent reviews (e.g. Ganias et al. (2014) and references therein) it has been demonstrated that using only the spawning capable females (for which energy for egg production is not a limiting factor), S estimates are quite consistent, i.e. females spawn with a specific biorythm in any particular ecosystem (the so called 'Hunter's biorhythm hypothesis'). For European anchovy, this inter-spawning interval has been estimated to be about 3 days (e.g. Schismenou et al., 2012; Uriarte et al., 2012). Hence, the value of $S = 0.33$, used in the present study is consistent with existing knowledge on species' spawning rhythm.

With regard to relative batch fecundity ($F/W$), laboratory and field evidence (reviewed in Ganias et al., 2014) indicate that this parameter is generally very conservative in anchovies and other species. Hence, the average value used here is likely the most appropriate estimate for relative batch fecundity of the NAS anchovy.

### Movement

Several approaches have been proposed in different ecosystems to simulate the movement of active fish stages within numerical models. In restricted-area search algorithms, a fitness function is defined first (Railsback et al., 1999). Given this function, individuals search the neighbouring cells and move towards the one that provides a locally optimal habitat. For example, Tu et al. (2012) simulated the spawning migration of Japanese anchovy under the hypotheses that fish swim along the current and change direction towards maximum temperature when sensing the optimal spawning temperature. The growth rate gradient was used to determine the fish behavioural movement of Peruvian anchovy (Xu et al., 2013) and Japanese sardine (Okunishi et al., 2012). Other approaches include the use of neural network genetic algorithms to direct movement (Huse and Ellingen, 2008; Okunishi et al., 2009) or adjusting the fish speed and frequency of turning angle as a response to a local habitat defined at the current fish position (Humston et al., 2004; Okunishi et al., 2012).

For the NAS ecosystem, broad scale migrations of anchovy have not been reported, possibly because it is an oligotrophic area and suitable, productive areas are spatially restricted (see 'Introduction' section). Furthermore, there is low inter-annual variability in the extent and location of anchovy habitats, as has been recorded and modelled from surveys at sea (Giannoulaki et al., 2008, 2013). It is thus most probable that anchovies do not perform extended horizontal migrations, limiting their movement in areas with sufficient amounts of food.

The movement module used in the IBM was based on food availability and bathymetry to simulate the displacement of active SIs. It was assumed that anchovy can move towards favorable feeding areas against the currents, maintaining a "known" bathymetric habitat that did not exceed some maximum water column depth. The latter (bathymetric) constraint on fish movement did not affect significantly the simulated anchovy distribution that was characterized by increased biomass in coastal, more productive areas, receiving river or BSW nutrient inputs. Overall, the movement algorithm produced outputs that were consistent with observed

distribution grounds of anchovy from acoustic surveys and statistical habitat maps estimated for anchovy in the NAS (Giannoulaki et al., 2008, 2013). In addition to trophic and bathymetric gradients, a function for slowing down the fish speed and a gradient based on local fish biomass were introduced in the movement module in order to prevent anchovy overcrowding in high prey areas. These two mechanisms were employed in an attempt to resolve the known problem of the restricted area search approach (Watkins and Rose, 2013), producing unrealistic spatial distribution patterns due to the aggregation of individuals in areas with high habitat quality. The sensitivity results presented in Section 'Movement' showed that the slowing down function was more effective to prevent the overcrowding of SIs, as compared to the density-dependent food gradient.

The present model simulated higher anchovy biomass and egg abundance in the inner Thermaikos Gulf, as compared to field data. This is possibly related to an overestimation of zooplankton by the LTL model in this area and/or the limitations of the implemented movement module, considering the shallow depth in this semi-enclosed area.

*Uncertainties/sensitivities of parameters*

Due to the high complexity of the coupled IBM system and the limited knowledge on many biological parameters, several types of uncertainties were inevitably included in the parameterization process. This is especially true for the natural mortalities, for which the values used were mainly based on figures or empirical relationships reported in past studies.

The half saturation parameter is the main calibrated parameter related to growth within bioenergetics models (Megrey et al., 2007; Pecquerie et al., 2009; Politikos et al., 2011). In the NAS, given the significant spatial variability of zooplankton (high in coastal areas influenced by rivers and low in offshore areas), the calibration of anchovy growth using only the half saturation parameter was not possible. Hence, a maximum in daily consumption was introduced, based on consumption rates observed for small pelagic species (Palomera et al., 2007; Nikolioudakis, 2011). This limitation in daily consumption was able to prevent high growth rates, especially in areas with noticeably increased plankton biomass like the river influenced area within the Thermaikos Gulf.

Another source of uncertainty in the IBM is the initialization of the fish model in terms of total biomass and location of the SIs. The anchovy model was initialized using available biomass data in June 2003. However, sensitivity simulations that initialized the anchovy model on a prior year (e.g. 2000), based on the same data as in 2003, did not show any significant changes as compared to the presented results for total biomass and anchovy distribution.

*Fishing*

In the IBM, the adopted fishing mortality was seasonal on a monthly basis and was applied homogeneously over the known NAS fishing grounds. This oversimplified parameterization restricted to some degree the spatial skills of the overall model. In the future, the integration of the spatiotemporal distribution of the fishing effort (purse seines) by elaboration and analysis of data from the vessel monitoring systems (*VMS*), as they become available, are expected to improve the model's performance in many ways. Firstly, the discrepancies between the observed and simulated distributions of fish biomass and egg abundance will be decreased. These discrepancies are partly due to the fact that, in coastal areas where the model predicts high concentrations of fish and their spawn, fishing effort is also very high, which is presently not explicitly included in the model. Also, the integration of the spatiotemporal distribution of the fishing effort will upgrade the model's performance by allowing for the simulation of spatiotemporal catch fields. Travers et al. (2007) have underlined the necessity of the representation of the simultaneous effects of fishing and climate within an end-to-end modelling approach for quantifying their propagation down and up the food web. Thus, the inclusion of an effective fishery module within our model is a necessary step to more realistically represent the fish distribution, as well as to use the model as a management tool in order to evaluate the effect of alternative management strategies scenarios (closed seasons, closed areas, different Total Allowance Catch levels) on the pelagic ecosystem. This is very important for the sustainable exploitation of anchovy resources in the NAS since the current technical measures applied in the area (2.5 month winter closed period, minimum legal landing sizes, etc.) are generally believed to be dated and inadequate whereas the stock is heavily exploited (Somarakis et al., 2006; Giannoulaki et al., 2014).

*Link between LTL and IBM model*

The two-way coupling between the fish and the LTL model allows the analysis of the role of the fish as a top down control agent, since zooplankton groups serve as prey fields for fish, which in turn induce predation mortality affecting the plankton dynamics (Travers et al., 2009). This interaction combined with nutrient feedback from fish by-products can play a key role on the general functioning of the pelagic food webs. For instance, Megrey et al. (2007) observed a small decrease in zooplankton biomass when a fish bioenergetics-based population dynamics model for Pacific herring was coupled with a biogeochemical model, as well as a small increase in phytoplankton, illustrating the interplay between the fish and the plankton model. In the southern Benguela ecosystem, Travers et al. (2009) performed a detailed comparison between two-way coupling versus one-way forcing of low and high trophic levels in an effort to scrutinize the role of fish predation in model coupling. The comparisons highlighted that the fish-induced plankton mortality and the top down feedback of the HTL to the LTL model affected not only the amplitude of the plankton dynamics but also the duration of the plankton bloom and caused small changes in ciliate and diatom biomass.

In this study, a similar approach was used and results were analyzed in two sub areas with quite different characteristics. In the mesotrophic Thracian Sea, an area with low enclosure, influenced both by riverine and BSW inputs, our results were in agreement with the previous studies (Megrey et al., 2007; Travers et al., 2009), showing a decrease in zooplankton and a relative increase of phytoplankton in the simulations with two-way coupling scheme. On the opposite, in the Thermaikos Gulf which is a semi-closed, eutrophic area the coupling of LTL model with fish, had a greater effect compared to the Thracian Sea, causing the decrease of phytoplankton, zooplankton and phosphate stocks. In eutrophic conditions, fish predation slows down the system in terms of primary producers (reduced production rate) and shifts the organic carbon towards the higher trophic levels.

## Conclusions

The coupling of physics and lower trophic levels to fish models that include all life stages, from eggs to adults, is not straightforward as in models restricted only to early life stages (Lett et al., 2009). However, it is an essential step for addressing issues related to the long-term consequences of climate and human-induced effects on fish populations and fisheries (Huse and Ellingen, 2008). Working within this context, the present work can be con-

**Table A.1**
Mathematical formulation of energy relationships and parameters values used to implement the anchovy bioenergetics model. Model structure and parameterization is basically adopted from Politikos et al. (2011).

| Energy process | Equations | Parameters |
|---|---|---|
| Maximum Consumption ($C_{max}$) | $C_{max} = a_c W_{SI}^{b_c} f_C(T)$ | $a_c$ = 0.41 (Intercept for consumption) |
| | | $b_c$ = −0.31 (Exponent for consumption) |
| | | $Q_c$ = 2.22[a,b], 2.4[c,d] (Slope for temperature dependence) |
| | | $T_{opt}$ = 20[a,b], 16[c,d] (Optimum Temperature (°C)) |
| | | $T_{max}$ = 32 (Maximum Temperature (°C)) |
| | $f_C(T) = V^X e^{X(1-V)}$ | $PD_{j,i}$ = density of prey type $i$ ($i$ = 1 corresponds to microzooplankton and $i$ = 2 to mesozooplankton) (g-prey $m^{-3}$) for life stage/age class $j$ |
| Temperature function | $V = \frac{T_{max}-T}{T_{max}-T_{opt}}$ | $v_{j,i}$ = vulnerability of prey type $i$ to life stage/age class $j$ (dimensionless) |
| | $S = (\ln Q_c)(T_{max} - T_{opt})$ | $v_{2,1}$ = 1.0, $v_{3,1}$ = 0.5 |
| | $Y = (\ln Q_c)(T_{max} - T_{opt} + 2)$ | $v_{4,1} = v_{5,1} = v_{6,1} = v_{7,1} = 0$, |
| | $X = \frac{S^2(1+(1+40/Y)^{1/2})^2}{400}$ | $v_{2,2} = 0.0$, $v_{3,2} = 0.5$, $v_{4,2} = v_{5,2} = v_{6,2} = v_{7,2} = 1.0$ |
| Consumption ($C$) | $C_i = \sum_{i=1}^{2} C_{j,i}$ | $k_{j,i}$ half saturation function (g-prey $m^{-3}$) for life stage $j$ feeding on prey type $i$. |
| | $C_{j,i} = \frac{C_{max}(PD_{j,i} v_{j,i}/k_{j,i})}{1+\sum_{i=1}^{2}(PD_{k,i} v_{k,i}/k_{k,i})}$ | $k_{2,1} = k_{2,2} = 0.016$, $k_{3,1} = k_{3,2} = 0.025$ |
| | | $k_{4,1} = k_{4,2} = 0.05$, $k_{5,1} = k_{5,2} = 0.09$ |
| | | $k_{6,1} = k_{6,2} = k_{7,1} = k_{7,2} = 0.1$ |
| Respiration ($R$) | $R = a_r W_{SI}^{b_r} f_R(T) A$ | $a_r$ = 0.024 (Intercept for respiration) |
| | $f_R(T) = Q_{10}^{\frac{T-T_m}{10}}$ | $b_r$ = −0.34 (Exponent for respiration) |
| | $A = e^{d_r U}$ | $Q_{10}$ = 2.22 Temperature dependence parameter |
| | $U = a_A W^{b_A} e^{(c_A T)}$ | $T_m$ = 18[a,b], 15[c,d] (Mean annual temperature) |
| | | $d_r$ = 0.022 (Coefficient for R for swimming speed) |
| | | $a_A$ = 2.0 (Intercept U (< 12.0 °C)) |
| | | $a_A$ = 12.25[a,b], 11.98[c], 14.21[d] (Intercept U (⩾ 12.0 °C)) |
| | | $a_A$ = 9.97[c] (Intercept U (⩾ 12.0 °C) (during low feeding activity) |
| | | $b_A$ = 0.27[a,b], 0.33[c], 0.27[d] (Coefficient U for weight) |
| | | $c_A$ = 0.149 (Coefficient U vs. temperature (< 12.0 °C)) |
| | | $c_A$ = 0.0 Coefficient U vs. temperature (⩾ 12.0 °C) |
| Egestion ($EG$) | $F = a_f C$ | $a_f$ = 0.15[a,b], 0.126[c,d] (Proportion of food egested) |
| Excretion ($EX$) | $E = a_e (C - F) + b_e$ | $a_e$ = 0.41 (Excretion coefficient) |
| | | $b_e$ = 0.01 (Proportion of food excreted) |
| Specific Dynamic Action ($SDA$) | $SDA = a_{sda}(C - F)$ | $a_{sda}$ = 0.10 (Specific dynamic action coefficient) |
| Energy buffer ($RE$) | See Section 'Reproduction' | |

[a] Early larval stage ($j$ = 2).
[b] Late larval stage ($j$ = 3).
[c] Juvenile stage ($j$ = 4).
[d] Adult age-classes ($j$ = 5,6,7).

sidered as a first attempt for the development of a holistic model scheme, which describes the main features of a small pelagic fish full life cycle, under the influence of trophic regimes provided by a coupled hydrodynamic–biogeochemical model.

Certainly, one has to keep in mind the mediations discussed in Rose (2012), who underlines the challenges, which will be faced in the future towards the improvement of model forecasting abilities. These challenges include scaling/computational issues, data needs, deciding what processes and organisms can be ignored and which ones must be represented. The present study gave us the opportunity to identify the associated uncertainties, combine the up to date biological information with new modelling theories (e.g. movement) and identify data gaps. The importance of developing methods for estimating the effect of these uncertainties in model predictions is an essential subsequent step.

The present model presents intermediate complexity. More fish species (e.g., sardine), top predators and fishing fleet modules can be added as knowledge on these components improves. The implemented egg production module can help to scrutinize the factors that can generate inter-annual variations in spawning patterns, a crucial step to understand the relationship between spawning and recruitment success. Finally, since the model presents in detail the plankton - fish interaction, it can be used for simulations investigating the impact of temperature rise, eutrophication and fresh waters inputs (river nutrient loads, Black Sea water) on the plankton productivity and subsequently on the anchovy dynamics.

## Acknowledgements

We would like to thank the reviewers for the very careful reading of our manuscript and their constructive comments. This work was financially supported by the General Secretariat of Research and Technology, Greece through the project REPROdUCE (REcruitment PROcesses Using Coupled biophysical models of the pelagic Ecosystem) – "Strengthening the links between European marine fisheries science and fisheries management – MARIFISH" (ERAC-CT-2006-025989) within the framework of the EU ERA-Net initiative (6th Framework Program), and the project SEAMAN (Spatially resolved Ecosystem Models and their Application to marine MANagement) – "Towards integrated European marine research strategy and programmes – SEAS-ERA" (ERAC-CT2009-249552) within

**Table A.2**
Mortality parameters used for the implementation of the population module.

| Parameter identification | Units | Parameter values |
|---|---|---|
| *Natural mortality ($M_{SI}$)* | | |
| Embryonic stage | $day^{-1}$ | 0.4 (Somarakis et al., 2012) |
| Early larval stage | $day^{-1}$ | Density-dependent (Somarakis and Nikolioudakis, 2007) |
| Late larval stage | $day^{-1}$ | 0.06 (Mantzouni et al., 2007) |
| Age-0 class | $year^{-1}$ | 4.0 (calibrated) |
| Age-1 class | $year^{-1}$ | 1.0 (Giannoulaki et al., 2014) |
| Age-2 class | $year^{-1}$ | 0.74 (Giannoulaki et al., 2014) |
| Age-3 class | $year^{-1}$ | 0.66 (Giannoulaki et al., 2014) |
| *Monthly Fishing mortality ($F_{month}$)* | | |
| Age-1, Age-2, Age-3 | $year^{-1}$ | 0.0, 0.0, 0.16, 0.44,0.75, 1.02, 1.26, 0.96, 0.52, 0.47, 0.35, 0.02 (Giannoulaki et al., 2014; unpublished HCMR data, see Fig. B.2) |

**Table A.3**
Parameters of the movement module.

| Parameters | Description | Value |
|---|---|---|
| $a_L$ | Maximum speed proportion factor | 1.7 ($s^{-1}$) |
| $R_L$ | Maximum degree of error | 0.25 ∗ fish-length |
| $k_z$ | Half-saturation parameter for slowing down the movement | 0.01 (mmol $N/m^3$) (calibrated) |
| $d_{wc}$ | Parameter which controls the steepness of the function FT | 100 (meters) (calibrated) |
| $\Delta t$ | Time step | 20 min |

**Table A.4**
Parameters of the fish distribution function.

| Parameter | Description | Value |
|---|---|---|
| $pref_4(j)$ | Preference on mesozooplankton | 0.5[a], 1.0[b] (dimensionless) (Nikolioudakis, 2011) |
| $pref_5(j)$ | Preference on microzooplankton | 0.5[a], 0.0[b] (dimensionless) (Nikolioudakis, 2011) |
| $k_f(j, food)$ | Vertical distribution steepness parameter | 50[a], 40[b] $(mgC/m^3)^2$ (calibrated) |
| ffc | Fish biomass conversion factor | 147(mgC/g ww)* |
| qnF | Fish C:N internal quota | 0.019 (mmol N/mgC)* |
| qpF | Fish C:P internal quota | 0.00136 (mmolP/mgC)* |
| qnZ5 | Z5 maximum N/C ratio | 0.0167 (mmol N/mgrC)** |
| qnZ4 | Z4 maximum N/C ratio | 0.015 (mmol N/mgrC)** |
| qpZ5 | Z5 maximum P/C ratio | 0.001 (mmolP/mgrC)** |
| qpZ4 | Z4 maximum P/C ratio | 0.00167 (mmolP/mgrC)** |

[a] Late larvae ($j = 3$).
[b] Age-0 to age-3 ($j = 4,5,6,7$).
* Czamanski et al. (2011).
** Petihakis et al. (2002).

the framework of the EU ERA-Net initiative (7th Framework Program). It was additionally supported by the European Union's 7th Framework Programme under grant agreement No. 283291, through the project "Operational Ecology" (OpEc). We thank Dr E. Schismenou for providing the length at age data for anchovy larvae.

## Appendix A

The equations and the parameters of the bioenergetics model are summarized in Table A.1. The list of parameters of the population module are shown in Table A.2. Table A.3 shows the parameters of the movement module, while the parameters of the coupling process are listed in Table A.4.

## Appendix B

See Figs. B.1 and B.2.

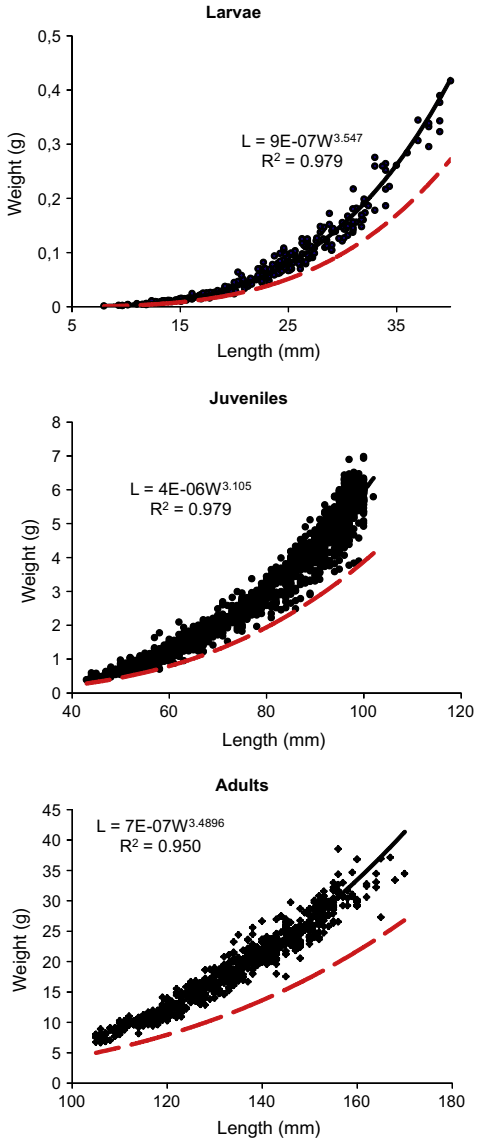


**Fig. B.1.** Length–weight relationships for anchovy larvae, juveniles and adults. The red lines indicate the −0.35 condition threshold. (For interpretation of the references to colour in this figure legend, the reader is referred to the web version of this article.)

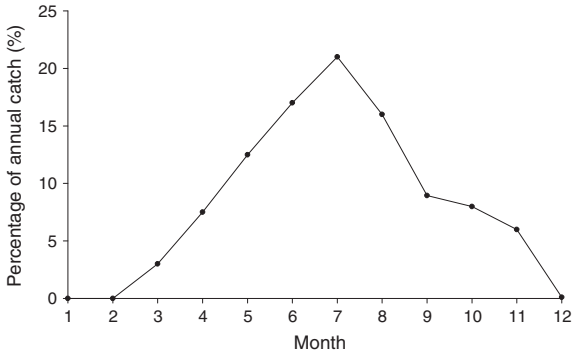


**Fig. B.2.** Mean monthly proportion of anchovy catch (percentage of annual catch) in the NAS for the period 2003–2006 (HCMR unpublished data).

## References


Agostini, V.N., Bakun, A., 2002. 'Ocean triads' in the Mediterranean Sea: physical mechanisms potentially structuring reproductive habitat suitability (with example application to European anchovy, *Engraulis encrasicolus*). Fisheries Oceanography 11, 129–142.

Alheit, J., Roy, C., Kifani, S., 2009. Decadal-scale variability in populations. In: Checkley, D. et al. (Eds.), Climate Change and Small Pelagic Fish. Cambridge University Press, pp. 64–87.

Allain, G., Petitgas, P., Lazure, P., 2007. The influence of environment and spawning distribution on the survival of anchovy (*Engraulis encrasicolus*) larvae in the Bay of Biscay (NE Atlantic) investigated by biophysical simulations. Fisheries Oceanography 16, 506–514.

Baretta, J.W., Ebenhoh, W., Ruardij, P., 1995. The European regional seas ecosystem model, a complex marine ecosystem model. Netherlands Journal of Sea Research 33, 233–246.

Blumberg, A.F., Mellor, G.L., 1983. Diagnostic and prognostic numerical circulation studies of the South Atlantic Bight. Journal of Geophysical Research: Oceans 88, 4579–4592.

Broekhuizen, N., Heath, M.R., Hay, S.J., Gurney, W.S.C., 1995. Modelling the dynamics of the North Sea's mesozooplankton. Netherlands Journal of Sea Research 33, 381–406.

Czamanski, M., Nugraha, A., Pondaven, P., Lasbleiz, M., Masson, A., Caroff, N., Bellail, R., Treguer, P., 2011. Carbon, nitrogen and phosphorus elemental stoichiometry in aquacultured and wild-caught fish and consequences for pelagic nutrient dynamics. Marine Biology 158, 2847–2862.

Edwards, A.M., Yool, A., 2000. The role of higher predation in plankton population models. Journal of Plankton Research 22, 1085–1112.

Fréon, P., Cury, P., Shannon, L., Claude, Roy C., 2005. Sustainable exploitation of small pelagic fish stocks challenged by environmental and ecosystem changes: a review. Bulletin of Marine Science 76, 385–462.

Fulton, E.A., 2010. Approaches to end-to-end ecosystem models. Journal of Marine Systems 81, 171–183.

Ganias, K., Somarakis, S., Nunes, C., 2014. Reproductive potential. In: Biology and Ecology of Sardines and Anchovies. CRC Press, Taylor & Francis Group, Boca Raton, pp. 79–121.

Giannoulaki, M., Valavanis, D.V., Palialexis, A., Tsagarakis, K., Machias, A., Somarakis, S., Papaconstantinou, C., 2008. Modelling the presence of anchovy *Engraulis encrasicolus* in the Aegean Sea during early summer, based on satellite environmental data. Hydrobiologia 612, 225–240.

Giannoulaki, M., Iglesias, M., Tugores, M.P., Bonanno, A., Patti, B., De Felice, A., Leonori, I., Bigot, J.L., Tičina, V., Pyrounaki, M.M., Tsagarakis, K., Machias, A., Somarakis, S., Schismenou, E., Quinci, E., Basilone, G., Cuttitta, A., Campanella, F., Miquel, J., Oñate, D., Roos, D., Valavanis, V., 2013. Characterizing the potential habitat of European anchovy *Engraulis encrasicolus* in the Mediterranean Sea, at different life stages. Fisheries Oceanography 22, 69–89.

Giannoulaki, M., Ibaibarriaga, L., Antonakakis, K., Uriarte, A., Machias, A., Somarakis, S., Sanchez, S., Roel, B.A., 2014. Applying a two-stage Bayesian dynamic model to a short lived species, the anchovy in the Aegean Sea (*Eastern Mediterranean*). Comparison with an Integrated Catch at Age stock assessment model. Mediterranean Marine Science 15, 350–365.

Hinrichsen, H.-H., Dickey-Collas, M., Huret, M., Peck, M.A., Vikebø, F.B., 2011. Evaluating the suitability of coupled biophysical models for fishery management. ICES Journal of Marine Science 68, 1478–1487.

Humston, R., Olson, D.B., Ault, J.S., 2004. Behavioural assumptions in models of fish movement and their influence on population dynamics. Transactions of the American Fisheries Society 133, 1304–1328.

Hunter, J.R., Leong, R., 1981. The spawning energetics of female northern anchovy, *Engraulis mordax*. Fishery Bulletin 79, 215–230.

Hunter, J.R., Macewicz, B., 1985. Rates of atresia in the ovary of captive and wild northern anchovy, *Engraulis mordax*. Fishery Bulletin 83, 119–136.

Huret, M., Petitgas, P., Woillez, M., 2010. Dispersal kernels and their drivers captured with a hydrodynamic model and spatial indices: a case study on anchovy (*Engraulis encrasicolus*) early life stages in the Bay of Biscay. Progress in Oceanography 87, 6–17.

Huse, G., Ellingen, I., 2008. Capelin migrations and climate change – a modelling analysis. Climatic Change 87, 117–197.

Ito, S.I., Okunishi, T., Michio, J., Kishi, M.J., Wang, M., 2013. Modelling ecological responses of Pacific saury (*Cololabis saira*) to future climate change and its uncertainty. ICES Journal of Marine Science. http://dx.doi.org/10.1093/icesjms/fst089.

Kavadas, S., Maina, I., 2012. Methodology of analysis of vessel monitoring system data: estimation of fishing effort for the fleet of open sea fishery. In: Proceedings of the 10th Panhellenic Symposium on Oceanography and Fisheries, 11pp.

Kourafalou, V., Tsiaras, K., 2007. A nested circulation model for the North Aegean, Sea. Ocean Science 3, 1–16.

Lasker, R. (Ed.), 1985. An egg production method for estimating spawning biomass of pelagic fish: application to the northern anchovy, *Engraulis mordax*. NOAA Tech. Rep. NMFS 36.

Lett, C., Rose, K.A., Megrey, B.A., 2009. Chapter 6: Biophysical models of small pelagic fish. In: Checkley, D.M., Alheit, J., Oozeki, Y., Roy, C. (Eds.), Climate Change and Small Pelagic Fish. Cambridge University Press, pp. 88–111.

Machias, A., Somarakis, S., Drakopoulos, P., Magoulas, A., Koutsikopoulos, C., 2000. Evaluation of the Southern Greek anchovy stocks. Project 97-0048. Final Report, 105 pp.

Mantzouni, I., Somarakis, S., Moutopoulos, D.K., Kallianiotis, A., Koutsikopoulos, C., 2007. Periodic, spatially structured matrix model for the study of anchovy (*Engraulis encrasicolus*) population dynamics in N Aegean Sea (*E. Mediterranean*). Ecological Modelling 208, 367–377.

McBride, R.S., Somarakis, S., Fitzhugh, G.R., Albert, A., Yaragina, N.A., Wuenschel, M.J., Alonso-Fernández, A., Basilone, G., 2014. Energy acquisition and allocation to egg production in relation to fish reproductive strategies. Fish and Fisheries. http://dx.doi.org/10.1111/faf.12043.

Megrey, B.A., Rose, K.A., Klumb, R.A., Hay, D.E., Werner, F.E., Eslinger, D.L., Smith, S.L., 2007. A bioenergetics-based population dynamics model of Pacific herring (*Clupea harengus pallasi*) coupled to a lower trophic level nutrient–phytoplankton–zooplankton model: description, calibration, and sensitivity analysis. Ecological Modelling 202, 144–164.

Mukai, D., Kishi, M.J., Ito, S.I., Kurita, Y., 2007. The importance of spawning season on the growth of Pacific saury: a model-based study using NEMURO, FISH. Ecological Modelling 202, 165–173.

Nikolioudakis, N., 2011. Trophic ecology of small pelagic fish. PhD thesis, Department of Biology, University of Crete, Greece, pp. 185.

Nikolioudakis, N., Isari, S., Somarakis, S., 2014. Trophodynamics of anchovy in a non-upwelling system: direct comparison with sardine. Marine Ecology Progress Series 500, 215–229.

Nittis, K., Perivoliotis, L., Korres, G., Tziavos, C., Thanos, I., 2006. Operational monitoring and forecasting for marine environmental applications in the Aegean Sea. Environmental Modelling and Software 21, 243–257.

Oguz, T., Salihoglu, B., Fach, B., 2008. A coupled plankton–anchovy population dynamics model assessing nonlinear controls of anchovy and gelatinous biomass in the Black Sea. Marine Ecology Progress Series 369, 229–256.

Okunishi, T., Yamanaka, Y., Ito, S.-I., 2009. A simulation model for Japanese sardine (*Sardinops melanostictus*) migrations in the western North Pacific. Ecological Modelling 220, 462–479.

Okunishi, T., Ito, S., Ambe, D., Takasuka, A., Kameda, T., Tadokoro, K., Setou, T., Komatsu, K., Kawabata, A., Kubota, H., Ichikawa, T., Sugisaki, H., Hashioka, T., Yamanaka, Y., Yoshie, N., Watanabe, T., 2012. A modeling approach to evaluate growth and movement for recruitment success of Japanese sardine (*Sardinops melanostictus*) in the western Pacific. Fisheries Oceanography 21, 44–57.

Olivar, M.P., Salat, J., Palomera, I., 2001. A comparative study of the spatial distribution patterns of the early stages of anchovy and pilchard in the NW Mediterranean Sea. Marine Ecology Progress Series 217, 111–120.

Palomera, I., Olivar, M.P., Salat, J., Sabatis, A., Coll, M., García, A., Morales-Nin, B., 2007. Small Pelagic Fish in the NW Mediterranean Sea: an ecological review. Progress in Oceanography 74, 377–396.

Papadopoulos, A., Kallos, G., Katsafados, P., Nickovic, S., 2002. The Poseidon weather forecasting system: an overview. The Global Atmosphere and Ocean Systems 8, 219–237 (retitled Journal of Atmospheric and Ocean Science).

Pecquerie, L., Petitgas, P., Kooijman, S.A., 2009. Modeling fish growth and reproduction in the context of the Dynamic Energy Budget theory to predict environmental impact on anchovy spawning duration. Journal of Sea Research 62, 93–105.

Pethybridge, H., Roos, D., Loizeau, V., Pecquerie, L., Bacher, C., 2013. Responses of European anchovy vital rates and population growth to environmental fluctuations: an individual-based modeling approach. Ecological Modelling 250, 370–383.

Petihakis, G., Triantafyllou, G., Allen, I.J., Hoteit, I., Dounas, C., 2002. Modelling the spatial and temporal variability of the Cretan Sea ecosystem. Journal of Marine Systems 36, 173–196.

Polat, C., Tugrul, S., Coban, Y., Basturk, O., Salihoglu, I., 1998. Elemental composition of seston and nutrient dynamics in the Sea of Marmara. Hydrobiologia 363, 157–167.

Politikos, D.V., Triantafyllou, G.N., Petihakis, G., Tsiaras, K., Somarakis, S., Ito, S.I., Megrey, B.A., 2011. Application of a bioenergetics growth model for European anchovy (*Engraulis encrasicolus*) linked with a lower trophic level ecosystem model. Hydrobiologia 670, 141–163.

Railsback, S.F., Lamberson, R.H., Harvey, B.C., Duffy, W.E., 1999. Movement rules for individual-based models of stream fish. Ecological Modelling 123, 73–89.

Rose, K.A., Werner, F.E., Megrey, B.A., Aita, M.N., Yamanaka, Y., Hay, D.E., Schweigert, J.F., Foster, M.B., 2007. Simulated herring growth responses in the Northeastern Pacific to historic temperature and zooplankton conditions generated by the 3-Dimensional NEMURO nutrient-phytoplankton-zooplankton model. Ecological Modelling 202, 184–195.

Rose, K.A., Allen, J.I., Artioli, Y., Barange, M., Blackford, J., Carlotti, F., Cropp, R.A., Daewel, U., Edwards, K., Flynn, K., Hill, S.L., HilleRisLambers, R., Huse, G., Mackinson, S., Megrey, B., Moll, A., Rivkin, R., Salihoglu, B., Schrum, C., Shannon, L., Shin, Y.J., Smith, S.L., Smith, C., Solidoro, C., John, M.S., Zhou, M., 2010. End-to-end models for the analysis of marine ecosystems: challenges, issues, and next steps. Marine and Coastal Fisheries 2, 115–130.

Rose, K.A., 2012. End-to-end models for marine ecosystems: are we on the precipice of a significant advance or just putting lipstick on a pig? Scientia Marina 76, 195–201.

Sabatés, A., Zaragoza, N., Grau, C., Salat, J., 2008. Vertical distribution of early developmental stages in two coexisting clupeoid species, *Sardinella aurita* and *Engraulis encrasicolus*. Marine Ecology Progress Series 364, 169–180.

Scheffer, M., Baveco, J.M., DeAngelis, D.L., Rose, K.A., 1995. Super-individuals: a simple solution for modelling large populations on an individual basis. Ecological Modelling 80, 161–170.

Schismenou, E., 2012. Modern approaches in biology and ecology of reproduction and growth of anchovy (*Engraulis encrasicolus*) in the North Aegean Sea. PhD thesis, University of Crete, Greece.

Schismenou, E., Somarakis, S., Thorsen, A., Kjesbu, O.S., 2012. Dynamics of de novo vitellogenesis in fish with indeterminate fecundity: an application of oocyte packing density theory to European anchovy, *Engraulis encrasicolus*. Marine Biology 159, 757–768.

Siokou-Frangou, I., Bianchi, M., Christaki, U., Christou, E.D., Giannakourou, A., Gotsis, O., Ignatiades, L., Pagou, K., Pitta, P., Psarra, S., Souvermezoglou, E., Van Wambeke, F., Zervakis, V., 2002. Carbon flow in the planktonic food web along a gradient of oligotrophy in the Aegean Sea (Mediterranean Sea). Journal of Marine Systems 33–34, 335–353.

Skoulikidis, N.Th., 2009. The environmental state of rivers in the Balkans – a review within the DPSIR framework. Science of the Total Environment 407, 2501–2516.

Smagorinsky, J., 1985. Prospects of atmospheric modelling and its impacts on weather prediction. In: Medium Range Weather Forecasts: The First 10 years, Proceedings of the 10th Anniversary of EMCWF, pp. 97–107.

Smith, A.D.M., Brown, C.J., Bulman, C.M., Fulton, E.A., Johnson, P., Kaplan, I.C., Lozano-Montes, H., Mackinson, S., Marzloff, M., Shannon, L.J., Shin, Y.J., Tam, J., 2011. Impacts of fishing low-trophic level species on marine ecosystems. Science 333 (6046), 1147–1150.

Somarakis, S., Nikolioudakis, N., 2007. Oceanographic habitat, growth and mortality of larval anchovy (*Engraulis encrasicolus*) in the northern Aegean Sea (eastern Mediterranean). Marine Biology 152, 1143–1158.

Somarakis, S., Nikolioudakis, N., 2010. What makes a late anchovy larva? the development of the caudal fin seen as a milestone in fish ontogeny. Journal of Plankton Research 32, 317–326.

Somarakis, S., Palomera, I., Garcia, A., Quintanilla, L., Koutsikopoulos, C., Uriarte, A., Motos, L., 2004. Daily egg production of anchovy in European waters. ICES Journal of Marine Science 61, 944–958.

Somarakis, S., Tsianis, D.E., Machias, A., Stergiou, K.I., 2006. An overview of biological data related to anchovy and sardine stocks in Greek waters. In: Palomares, M.L.D., Stergiou, K.I., Pauly, D. (Eds.), Fishes in Databases and Ecosystems. Fisheries Centre Research Reports, vol. 14(4). Fisheries Centre, University of British Columbia, pp. 56–64.

Somarakis, S., Schismenou, E., Siapatis, A., Giannoulaki, M., Kallianiotis, A., Machias, A., 2012. High variability in the Daily Egg Production Method parameters of an eastern Mediterranean anchovy stock: influence of environmental factors, fish condition and population density. Fisheries Research 117–118, 12–21.

Stergiou, K.I., Christou, E.D., Georgopoulos, D., Zenetos, A., Souvermezoglou, C., 1997. The Hellenic Seas: physics, chemistry, biology and fisheries. Oceanography and Marine Biology: Annual Review 35, 415–538.

Taylor, K.E., 2001. Summarizing multiple aspects of model performance in a single diagram. Journal of Geophysical Research: Atmospheres 106, 7183–7192.

Travers, M., Shin, Y.-J., Jennings, S., Cury, P., 2007. Towards end-to-end models for investigating the effects of climate and fishing in marine ecosystems. Progress in Oceanography 75, 751–770.

Travers, M., Shin, Y.-J., Jennings, S., Machu, E., Huggett, J.A., Field, J.G., Cury, P.M., 2009. Two-way coupling versus one-way forcing of plankton and fish models to predict ecosystem changes in the Benguela. Ecological Modelling 220, 3089–3099.

Tsiaras, K., Korres, G., Petihakis, G., Nittis, K., Raitsos, D., Pollani A., Triantafyllou, G., 2010. The Poseidon ecosystem model: the Mediterranean case. In: Proceedings of the 5th International Conference of EuroGOOS, EuroGOOS publication n. 28, 191–198, ISBN: 978-91-974828-6-8.

Tsiaras, K., Kourafalou, V., Raitsos, D., Triantafyllou, G., Petihakis, G., Korres, G., 2012. Inter-annual productivity variability in the North Aegean Sea: influence of thermohaline circulation during the Eastern Mediterranean Transient. Journal of Marine Systems 96–97, 72–81.

Tsiaras, K., Petihakis, G., Kourafalou, V., Triantafyllou, G., 2014. Impact of the river nutrient load variability on the *N. Aegean* ecosystem functioning over the last decades. Journal of Sea Research 86, 97–109.

Tu, C.Y., Tseng, Y.E., Chiu, T.S., Shen, M.L., Hsieh, C.H., 2012. Using coupled fish behaviour-hydrodynamic model to investigate spawning migration of Japanese anchovy, *Engraulis japonicus*, from the East China Sea to Taiwan. Fisheries Oceanography 21, 255–268.

Tudela, S., Palomera, I., 1999. Potential effect of an anchovy-mediated pump on the vertical availability of nitrogen for primary production in the Catalan Sea (northwest Mediterranean). Journal of Sea Research 42, 83–92.

Tugrul, S., Besiktepe, S.T., Salihoglou, I., 2002. Nutrient exchange fluxes between the Aegean and Black Seas through the Marmara Sea. Mediterranean Marine Science 3, 33–42.

Uriarte, A., Prouzet, P., Villamor, B., 1996. Bay of Biscay and Ibero Atlantic anchovy populations and their fisheries. Scientia Marina 60, 237–255.

Uriarte, A., Alday, A., Santos, M., Motos, L., 2012. A re-evaluation of the spawning fraction estimation procedures for Bay of Biscay anchovy, a species with short interspawning intervals. Fisheries Research 117–118, 96–111.

Valdés, E.S., 1993. The energetics and evolution of intraspecific predation (egg cannibalism) in the anchovy *Engraulis capensis*. Marine Biology 115, 301–330.

Wang, Y., Wei, H., Kishi, M.J., 2013. Coupling of an individual-based model of anchovy with lower trophic level and hydrodynamic models. Journal of Ocean University of China 12 (1), 45–52.

Watkins, K.S., Rose, K.A., 2013. Evaluating the performance of individual-based animal movement models in novel environments. Ecological Modelling 250, 214–234.

Xu, Y., Chai, F., Rose, K.A., Ñiquen, C.M., Chavez, F.P., 2013. Environmental influences on the interannual variation and spatial distribution of Peruvian anchovy (*Engraulis ringens*) population dynamics from 1991 to 2007: a three-dimensional modeling study. Ecological Modelling 264, 64–82.